

The Security Budget of Code-LLM Prompt Hardening: Provable Limits Under Pass-Only Acceptance

Jianwei Tai

School of Internet, Anhui University
24012@ahu.edu.cn

Abstract

We give a quantitative impossibility result for pass-only prompt hardening of code LLMs. For any deterministic prompt filter h and a registered family of finite executable-equivalence task variables $\mathcal{Y}_{\text{exec}}$, the shared filtered-prompt channel $I(h(p); h(\tilde{p}))$ is lower-bounded by a worst- Y Fano floor; on HumanEval and MBPP the universal pass-only floor evaluates to $\mathcal{F}^{\text{op}} \geq 0.84$ and 1.20 nats at $\eta = 0.05$ task-collapse tolerance, and the identity row realizes $\mathcal{F}^{\text{id}} \geq 1.67$ and 1.80 nats. An estimator-invariance corollary lifts the floor to any deterministic embedding pipeline; a dataset-agnostic corollary states the floor in visible-spec entropy and is empirically witnessed by 164/164 HumanEval+ and 224/224 MBPP+ $V(p)$ -invariance. We operationalize the floor as the *Tri-Audit Protocol*, a two-axis reporting protocol that separates a prompt-side deductive registry attribute (Shannon nats on the visible-spec representation) from a model-side empirical proxy (KSG-1 primary, MINE secondary, on hidden states). A constrained best-of-family search over deterministic and guarded learned filters on CodeLlama-7B, Qwen2.5-Coder-7B/1.5B and DeepSeek-Coder-6.7B at $n = 164$ yields the *Cross-Model Tri-Audit Invariance*: of twenty-eight pass-preserving rows, twelve antecedent-preserving deterministic rows fail proxy-axis leakage reduction on every backbone with sign-invariant positive deviations, twelve antecedent-changed-of-record learned-canonicalizer rows fail proxy-axis leakage on every backbone, and four antecedent-violating rows are reported as registered-family collapse; no filter produces a shared Tri-pass on a nine-cell gate-sensitivity sweep. Pass@1 alone cannot certify code-LLM prompt hardening. The residue is quantitative, and the visible-spec leg is load-bearing: dropping it admits a registered-family collapse attack that the proxy gate alone would let through.

1 Introduction

Code LLMs such as CodeLlama, Qwen2.5-Coder, and DeepSeek-Coder (Guo et al. 2024) now sit inside programming-assistant workflows. Developers steer implementations with natural-language prompts, examples, comments, and constraints. Small prompt perturbations can preserve the visible programming task while changing the generated implementation. The difficult case for evaluation is not an obviously corrupted prompt, but a benign-looking

edit: synonym substitution, identifier renaming, comment injection, or a security-directed suggestion that leaves the unit test interface intact.

Most code-generation evaluations reduce this question to execution pass rates before and after perturbation. Pass@1 is necessary: a filter that destroys the task is not a useful defense. It is also incomplete. A prompt filter may keep the task recognizable while leaving most perturbation information available; another may suppress the prompt channel only by deleting examples or semantic constraints that the model needs. A hardening audit therefore needs three quantities at once: a task-preservation screen, a filtered prompt-channel leakage measurement, and a clean-perturbed output-retention measurement.

We formalize this audit view with two information quantities:

- **Capacity** $\text{Cap} = I(c^*; c_\pi)$, the mutual information between the canonical solution c^* and the model’s generation c_π . This measures *how much of the task the model captures*.
- **Retention** $\text{Sec} = I(c_\pi; \tilde{c}_\pi)$, the mutual information between the model’s generation under the original prompt p and under an adversarially-perturbed prompt \tilde{p} . We keep the symbol Sec for continuity with the Cap-Sec budget, but throughout the paper it denotes clean-perturbed retention, not exploit success or vulnerable-code generation.

The main formal object is a quantitative impossibility result for pass-only prompt-hardening rules. For any deterministic filter h and a registered family $\mathcal{Y}_{\text{exec}} = \{Y_k = g_k(C)\}$ of finite executable-equivalence task variables, Fano’s inequality forces $I(h(p); h(\tilde{p})) \geq \sup_{Y_k} \{H(Y_k) - 2\phi_{M_k}(\delta_h(Y_k))\}$ whenever each Y_k is decodable from clean and perturbed filtered prompts, and an estimator-invariance corollary lifts the same lower bound onto every deterministic embedding pipeline used by an MI estimator. Under a pass-only acceptance rule with task-collapse tolerance η , this Fano floor is strictly positive: the universal pass-only floor (lower-bounding every pass-only-accepted filter) is $\mathcal{F}^{\text{op}} \geq 0.84$ nats on HumanEval and 1.20 nats on MBPP at $\eta = 0.05$, and the identity-filter row realizes $\mathcal{F}^{\text{id}} \geq 1.67$ and 1.80 nats (Theorem 5, Corollary 6). The companion Cap-Retention inequality, $\text{Cap} + \text{Sec} \leq H(c^*) + I(p; \tilde{p})$, supplies

the hidden-state ledger used for the output side of the audit. Across six individual embedded rows, the estimator-level check $(\text{Cap} + \max_T \text{Sec}) / (\text{H}(z^*) + \max_T \text{I}(p; \tilde{p}))$ ranges from 0.27 to 0.92, with positive estimator residuals, and diagnostic stress cells across a 23-perturbation pool and a gradient-based PGD pass remain inside the same diagnostic region.

Contributions.

1. **Quantitative pass-only hardening impossibility.** A worst- Y Fano-floor theorem (Theorem 5) over a registered family of executable-equivalence task variables: any pass-only acceptance rule with task-collapse tolerance η leaves a shared filtered-prompt residue of at least $\sup_{Y_k} \{\text{H}(Y_k) - 2\phi_{M_k}(\delta_0 + \eta)\}$, evaluating to $\mathcal{F}^{\text{op}} \geq 0.84$ and 1.20 nats on HumanEval and MBPP at $\eta = 0.05$. An estimator-invariance corollary lifts the floor to any deterministic embedding pipeline; a dataset-agnostic corollary states the floor in visible-spec entropy and M_V alone, witnessed empirically by 164/164 HumanEval+ and 224/224 MBPP+ $V(p)$ -invariance.
2. **Tri-Audit Protocol with two-axis reporting and four-mode failure coverage.** We instantiate the floor as the *Tri-Audit Protocol* (Definition 3), a two-axis reporting protocol that separates a prompt-side deductive registry attribute (Shannon nats on the visible-spec representation, automatically inherited from the Fano floor under the antecedent) from a model-side empirical proxy (KSG-1 primary, MINE secondary, on hidden states). The four conditions (pass@1, visible-spec antecedent, proxy leakage reduction, retention non-increase) cover four mutually distinguishable failure modes in the audited family (Proposition 1: capacity-loss, registered-family collapse, trivial filter, Pareto-degenerate retention inflation), each independently load-bearing.
3. **Cross-Model Tri-Audit Invariance over deterministic and learned filters.** A constrained best-of-family search on CodeLlama-7B, Qwen2.5-Coder-7B/1.5B, and DeepSeek-Coder-6.7B at $n = 164$ yields the empirical Cross-Model Tri-Audit Invariance: among twenty-eight pass-preserving rows on the primary slate (three pretraining families, Qwen-Coder at two scales, $4.7\times$ scale ratio), twelve antecedent-preserving deterministic rows fail proxy-axis leakage reduction with sign-invariant positive deviations on every backbone, twelve antecedent-changed-of-record learned-canonicalizer rows fail proxy-axis leakage on every backbone, four antecedent-violating rows are registered-family collapse; StarCoder2-7B at $n = 50$ replicates the partition. No filter produces a shared Tri-pass on a nine-cell gate-sensitivity sweep, and a task-blocked residual-leakage classifier separates total-channel semantics from perturbation identity.

The DPI inequality uses standard mutual-information monotonicity and data processing as a ledger for the audit. The main claim is the combination of a task-preserving filter theorem, a calibrated fixed-proxy audit policy, and the empirical finding that pass@1-preserving prompt filters

can fail the leakage/retention frontier even when a residual perturbation-leakage audit separates task semantics from perturbation identity.

This gives a practical test for prompt-level defenses: reducing $\text{I}(p; \tilde{p})$ tightens the maximum clean-perturbed information channel available to perturbations, but does not by itself increase Cap. Programming-assistant guardrails should be evaluated both by pass@1 and by the prompt-perturbation information they leave available to an adversary.

2 Related Work

Information-theoretic bounds and MI estimation. The information bottleneck line studies compression-prediction trade-offs in representations (Tishby, Pereira, and Bialek 2000; Tishby and Zaslavsky 2015), invariance and nuisance information (Achille and Soatto 2018), and MI-based representation learning (Hjelm et al. 2019). Empirical MI can be estimated by KSG (Kraskov, Stögbauer, and Grassberger 2004), MINE (Belghazi et al. 2018), or contrastive bounds such as InfoNCE (van den Oord, Li, and Vinyals 2018). Closer to our formal object, Gao et al. (Gao et al. 2025) use Fano’s inequality to upper-bound LLM accuracy as a function of task complexity in single-pass multi-hop QA; we differ in modality (code generation under unit tests), in channel (prompt-perturbation shared information $\text{I}(h(p); h(\tilde{p}))$), and in object (a worst- Y Fano floor on filtered-prompt leakage paired with a Cap-Retention sum $\text{Cap} + \text{Sec} \leq \text{H}(c^*) + \text{I}(p; \tilde{p})$ rather than a single-axis accuracy ceiling). These works measure or optimize information in a representation; our bound constrains a joint task-level sum, pairing faithfulness to canonical code with stability under prompt perturbation and a source-coding entropy ceiling (Cover and Thomas 2006).

Robustness of code LLMs and programming assistants. AI programming assistants make natural-language prompts both interface and attack surface. ReCode (Wang et al. 2023), NLPerturbator (Chen et al. 2024), ADVPRO (Li et al. 2024), CodeFort (Zhang et al. 2024), Operational Robustness (Paul, Zhu, and Bayley 2026), and Code Roulette (Paley et al. 2025) study code-generation robustness under prompt/code perturbations, prompt variability, or robust training. EvalPlus (Liu et al. 2023) tightens execution-based evaluation beyond HumanEval (Chen et al. 2021), while CodeBERTScore (Zhou et al. 2023) gives a continuous code-similarity signal. Recent AAAI work on RobustAPI (Zhong and Wang 2024) and CodeHalu (Tian et al. 2025) studies nearby reliability failures. Prompt-sensitivity and prompt-injection defenses such as PSM (Jawad and Brunel 2025) and recent defense evaluations (Deep et al. 2026) optimize or benchmark interventions directly. These papers measure, attack, improve, or defend prompt robustness; our audit instead asks whether pass-preserving filters also reduce a predeclared prompt-leakage/output-retention proxy gate.

Adversarial attacks and code security. GCG (Zou et al. 2023), PromptAttack (Xu et al. 2024), JailbreakBench

(Chao et al. 2024), worst-prompt evaluation (Cao et al. 2024), and single-character alignment failures (Lin et al. 2025) show that LLM behavior can be sensitive to adversarial prompt variation; PGD-style optimization (Madry et al. 2018) motivates our embedding-space stress test. Code-security work studies vulnerable generated code (Pearce et al. 2022), SecurityEval (Siddiq and Santos 2022), and secure code generation/adversarial testing (He and Vechev 2023). Kaneko et al. (Kaneko and Baldwin 2025) bound adversarial inference leakage per query. Our setting is orthogonal: a single-shot Cap+Sec budget for code generation under explicit $H(c^*)$ and $I(p; \tilde{p})$ terms.

Code naturalness and compressibility. Source code is statistically regular and compressible (Hindle et al. 2012; Karampatsis et al. 2020; Allamanis et al. 2018). We use this fact not as a language-modeling objective, but as a training-data-free upper bound on canonical-solution entropy and therefore on the Cap-Sec budget.

3 Theoretical Framework

3.1 Setup

Let p be a prompt drawn from a distribution \mathcal{D}_p , and let $c^* : p \mapsto c^*(p)$ be the (latent) canonical solution. Let $\pi(c | p)$ be a code LLM, and let $c_\pi \sim \pi(\cdot | p)$. An attacker maps p to a perturbed prompt $\tilde{p} \sim T(\cdot | p)$ where T is a perturbation kernel respecting an information budget $I(p; \tilde{p}) \leq B$. The model regenerates $\tilde{c}_\pi \sim \pi(\cdot | \tilde{p})$.

Definition 1 (Capacity and Retention).

$$\text{Cap}(\pi) := I(c^*; c_\pi), \quad (1)$$

$$\text{Sec}(\pi, T) := I(c_\pi; \tilde{c}_\pi). \quad (2)$$

We additionally posit the following technical condition, which holds for stateless offline evaluation when each prompt is decoded independently. It excludes shared-randomness evaluation, retrieval-augmented or tool-using systems with persistent state, batched inference artifacts that couple samples, and interactive assistant workflows that update memory between the clean and perturbed generations.

Benchmark-audit setting. The Cap-Retention inequality targets the setting in which prompt-hardening claims are usually benchmarked: the clean and perturbed generations are independently sampled from a stateless decoder given their prompts. This makes the bound observable in ordinary offline code-generation evaluations and isolates the prompt channel being audited. Systems with retrieval state, tool traces, shared caches, persistent assistant memory, or coupled batch effects introduce additional channels that should be audited separately rather than folded into the prompt-only ledger.

Definition 2 (Independence assumption). $c_\pi \perp \tilde{c}_\pi | (p, \tilde{p})$: given the prompt pair, the two generations are independent. This is the standard assumption that a stateless decoder makes for non-interactive evaluation.

3.2 Main Theorem

Theorem 1 (Capacity-Retention Diagnostic Inequality). *Let c^* be the canonical solution random variable (a deterministic function of p), c_π the model’s generation under p , and \tilde{c}_π the model’s generation under perturbed prompt \tilde{p} . Assume $c_\pi \perp \tilde{c}_\pi | (p, \tilde{p})$ (independent sampling, given the prompt pair). Then*

$$\text{Cap}(\pi) + \text{Sec}(\pi, T) \leq H(c^*) + I(p; \tilde{p}). \quad (3)$$

Proof. We bound each term separately.

(i) $\text{Cap} = I(c^*; c_\pi) \leq H(c^*)$ holds for any random variable c_π by the elementary identity $I(X; Y) = H(X) - H(X | Y) \leq H(X)$ (cf. Xu and Raginsky (Xu and Raginsky 2017) for an analogous use in IT-generalization analysis).

(ii) $\text{Sec} = I(c_\pi; \tilde{c}_\pi) \leq I(p; \tilde{p})$. The perturbation kernel observes the prompt but not the decoder randomness, so the joint sampling law factorizes as $\mathcal{D}(p)T(\tilde{p} | p)\pi(c_\pi | p)\pi(\tilde{c}_\pi | \tilde{p})$. This gives the Markov chain $c_\pi \rightarrow p \rightarrow \tilde{p} \rightarrow \tilde{c}_\pi$. By data processing, $I(c_\pi; \tilde{c}_\pi) \leq I(p; \tilde{p})$. Adding (i) and (ii) gives $\text{Cap} + \text{Sec} \leq H(c^*) + I(p; \tilde{p})$. Full proof of the chain in (ii), with explicit σ -algebras, is provided in the supplementary material.

Corollary 1 (Embedded-Variable Bound). *Let E be any deterministic embedding map applied to generated code, and let $z^* = E(c^*)$, $z_\pi = E(c_\pi)$, and $\tilde{z}_\pi = E(\tilde{c}_\pi)$. Under the assumptions of Theorem 1,*

$$I(z^*; z_\pi) + I(z_\pi; \tilde{z}_\pi) \leq H(z^*) + I(p; \tilde{p}). \quad (4)$$

Proof. Since E is deterministic, z^* is a deterministic function of p , z_π is sampled through p , and \tilde{z}_π is sampled through \tilde{p} . The same factorization as Theorem 1 gives $z_\pi \rightarrow p \rightarrow \tilde{p} \rightarrow \tilde{z}_\pi$, and the proof repeats with $(z^*, z_\pi, \tilde{z}_\pi)$ in place of $(c^*, c_\pi, \tilde{c}_\pi)$.

3.3 Closed-Form Companion Bound

Theorem 1 is only useful if the task-entropy term $H(c^*)$ can be bounded without access to the evaluated model. In code generation, the canonical solution is a token sequence, so source coding already gives an upper bound on its entropy.

Theorem 2 (Closed-Form Code-Specific Entropy Bound). *Let \mathcal{V} be a tokenizer vocabulary of size V , let L_{\max} be the maximum canonical-solution token length over the task distribution, and let $\overline{|c^*|_{\text{gz}}}$ be the expected gzip file-stream length of canonical solutions, including gzip framing bytes and measured in nats. Then*

$$H(c^*) \leq \min(L_{\max} \log V, \overline{|c^*|_{\text{gz}}}). \quad (5)$$

Proof sketch. A random variable supported on sequences of length at most L_{\max} over an alphabet of size V has entropy at most $L_{\max} \log V$. For the second term, any fixed lossless compressor induces a uniquely decodable code-length random variable, and expected code length upper-bounds source entropy up to the compressor’s fixed framing overhead. We use gzip as a reproducible conservative compressor and report its length in nats. Taking the smaller of the vocabulary-counting bound and the gzip-length bound gives Eq. (5).

On HumanEval canonical solutions, this gives $H(c^*) \leq 1739$ nats for both CodeLlama and Qwen-Coder tokenizers (numerical details in supplementary material). This closed-form ceiling is much looser than the empirical embedding estimate but is model-agnostic and training-data-free.

3.4 Interpretation

The bound saturates ($\text{Cap} + \text{Sec} = H(c^*) + I(p; \tilde{p})$) only when (a) c_π is a deterministic function of c^* (Cap saturates at $H(c^*)$) AND (b) \tilde{c}_π is a deterministic function of \tilde{p} that retains all prompt-leakage information (Sec saturates at $I(p; \tilde{p})$). Otherwise the gap measures unused channel budget: how much functional learning or generation stability remains before the bound is exhausted.

3.5 Prompt Filters as Diagnostic Controls

Corollary 2 (Deterministic Prompt Filters). *Let h be any deterministic prompt filter and define $c_\pi^h \sim \pi(\cdot | h(p))$ and $\tilde{c}_\pi^h \sim \pi(\cdot | h(\tilde{p}))$. Under the independence condition of Theorem 1,*

$$\text{Cap}_h + \text{Sec}_h \leq H(c^*) + I(h(p); h(\tilde{p})) \leq H(c^*) + I(p; \tilde{p}). \quad (6)$$

The first inequality applies Theorem 1 to the filtered prompt channel. The second follows from data processing because h is deterministic for the raw prompt variables. The corollary does not say that filtering improves task performance, nor does it imply that finite-sample hidden-state/MINE estimates must decrease across different filtered embedding distributions.

Theorem 3 (Task-Preservation Lower Bound for Prompt Filters). *Let $A = h(p)$ and $B = h(\tilde{p})$ be any two filtered prompt variables, and let $C = c^*$ be the task variable. Then*

$$\begin{aligned} I(A; B) &\geq I(A; C) + I(B; C) - H(C) & (7) \\ &= H(C) - H(C | A) - H(C | B). & (8) \end{aligned}$$

Consequently, if $H(C | A) \leq \epsilon_A$ and $H(C | B) \leq \epsilon_B$, then

$$I(h(p); h(\tilde{p})) \geq H(c^*) - \epsilon_A - \epsilon_B. \quad (9)$$

Proof. No Markov or independence assumption is needed. Entropy submodularity applied to sets (A, C) and (B, C) gives $H(A, C) + H(B, C) \geq H(C) + H(A, B, C)$. Monotonicity gives $H(A, B, C) \geq H(A, B)$, hence

$$H(A, C) + H(B, C) \geq H(C) + H(A, B). \quad (10)$$

Let

$$\begin{aligned} D &:= I(A; B) - I(A; C) \\ &\quad - I(B; C) + H(C). \end{aligned} \quad (11)$$

Expanding the mutual informations gives

$$\begin{aligned} D &= H(A, C) + H(B, C) \\ &\quad - H(A, B) - H(C). \end{aligned} \quad (12)$$

By Eq. (10), $D \geq 0$. This proves the lower bound in Eq. (8). The equality form follows from $I(A; C) = H(C) - H(C | A)$ and $I(B; C) = H(C) - H(C | B)$; Eq. (9) substitutes the two conditional-entropy bounds.

Theorem 4 (Pass-Only Hardening Has No Certificate). *Fix a prompt filter h and a task variable C . Consider any proposed prompt-hardening rule that accepts h from a task-collapse screen alone, for example because clean pass@1 changes by at most a declared tolerance. Such a rule is not a certificate of prompt hardening: if the filtered clean and perturbed prompts both retain the task, in the sense that $H(C | h(p)) \leq \epsilon_A$ and $H(C | h(\tilde{p})) \leq \epsilon_B$, then*

$$I(h(p); h(\tilde{p})) \geq H(C) - \epsilon_A - \epsilon_B. \quad (13)$$

Thus a pass-only rule can accept filters that provably retain a nonzero shared filtered-prompt channel. A hardening audit must also require evidence that the filtered prompt channel and the clean-perturbed generation-retention channel move down.

Proof. Equation (13) is Theorem 3 with $A = h(p)$ and $B = h(\tilde{p})$. The criterion follows because a pass-only rule observes only the task-collapse screen and can therefore accept a filter even when the lower bound leaves a large shared filtered-prompt channel. Corollary 2 supplies the companion output-retention ledger for the model generations, so a hardening audit must measure both prompt-side leakage and generation-side retention.

The theorem is the falsifiable consequence used in the experiments. DPI alone upper-bounds how much retention can pass through a prompt channel; it does not say when a pass-preserving filter should be rejected. The no-certificate theorem supplies the missing rejection condition: if the filter still preserves the task, then shared filtered-prompt information should remain, and a successful hardening claim must show that the measured leakage and retention proxies move down rather than relying on pass@1 alone. A filter can lower measured prompt content by discarding task information, but that movement should appear as capacity loss. The theorem is stated in terms of conditional task entropy, not execution accuracy. The next corollary gives the formal bridge used to interpret pass-style evidence after the task variable is coarsened to a finite executable class.

Corollary 3 (Executable-Equivalence Filter Lower Bound).

Let $Y = g(C)$ be a finite executable-equivalence task variable with $M = |\mathcal{Y}| \geq 2$ classes, and let $A = h(p)$ and $B = h(\tilde{p})$. Suppose there exist decoders $\hat{Y}_A(A)$ and $\hat{Y}_B(B)$ with error probabilities $P[\hat{Y}_A \neq Y] \leq \delta_A$ and $P[\hat{Y}_B \neq Y] \leq \delta_B$, where $0 \leq \delta_A, \delta_B < 1 - 1/M$. Then

$$I(A; B) \geq H(Y) - \phi_M(\delta_A) - \phi_M(\delta_B), \quad (14)$$

where $\phi_M(\delta) = h_2(\delta) + \delta \log(M - 1)$ and h_2 is binary entropy.

Proof. Fano's inequality gives $H(Y | A) \leq h_2(\delta_A) + \delta_A \log(M - 1)$ and $H(Y | B) \leq h_2(\delta_B) + \delta_B \log(M - 1)$. Applying Theorem 3 to the task variable Y gives $I(A; B) \geq H(Y) - H(Y | A) - H(Y | B)$, and substituting the two Fano bounds yields Eq. (14).

Corollary 3 is a positive-control certificate for a chosen finite executable variable. It does not identify HumanEval

pass@1 with $H(C | h(p))$, and the visible-example variable used below is not the same object as hidden-test correctness. The formal statement says only that, if an executable-equivalence variable can be decoded from filtered prompts with low error, then filters that preserve that variable inherit a shared-information lower bound for that variable. In the experiments, pass@1 remains empirical evidence outside the theorem: it screens for task collapse, while the Fano cell shows that at least one visible executable specification retained by near-identity filters has a nonzero shared-information certificate. A filter that preserves pass@1 but leaves the measured leakage channel high is therefore an empirical Pareto failure under the declared proxy gate; a filter that lowers content by collapsing pass@1 is a capacity-loss control rather than a successful defense.

Theorem 5 (Quantitative Pass-Only Hardening Impossibility). *Fix a registered family $\mathcal{Y}_{\text{exec}} = \{Y_k = g_k(C)\}_{k=1}^K$ of finite executable-equivalence task variables, where each Y_k has $M_k \geq 2$ classes and entropy $H(Y_k)$. For each k define $\phi_{M_k}(\delta) := h_2(\delta) + \delta \log(M_k - 1)$, where h_2 is the binary entropy. Let h be any deterministic prompt filter, and let $\delta_h(Y_k)$ denote the worst clean/perturbed decoder error $\max(\delta_A^{(k)}, \delta_B^{(k)})$ for Y_k from the filtered prompts $h(p), h(\tilde{p})$, where $\delta_A^{(k)}, \delta_B^{(k)} < 1 - 1/M_k$. Then*

$$I(h(p); h(\tilde{p})) \geq \sup_{Y_k \in \mathcal{Y}_{\text{exec}}} \{H(Y_k) - 2\phi_{M_k}(\delta_h(Y_k))\}. \quad (15)$$

Let $\delta_h^{\max}(\mathcal{Y}_{\text{exec}}) := \sup_{Y_k} \delta_h(Y_k)$. If a pass-only acceptance rule certifies that h preserves task collapse with tolerance η in the sense that $\delta_h^{\max}(\mathcal{Y}_{\text{exec}}) \leq \delta_0 + \eta$ for a clean baseline δ_0 (uniformly across $\mathcal{Y}_{\text{exec}}$), then

$$I(h(p); h(\tilde{p})) \geq \mathcal{F}(\delta_0, \eta; \mathcal{Y}_{\text{exec}}) := \sup_{Y_k} \{H(Y_k) - 2\phi_{M_k}(\delta_0 + \eta)\}, \quad (16)$$

which is strictly positive whenever some Y_k satisfies $\phi_{M_k}(\delta_0 + \eta) < \frac{1}{2}H(Y_k)$. Reducing the shared filtered-prompt channel below \mathcal{F} requires raising the worst decoder error toward $1 - 1/M_k$ on every registered coarsening, i.e. collapsing $\mathcal{Y}_{\text{exec}}$.

Proof. For each $Y_k \in \mathcal{Y}_{\text{exec}}$, Corollary 3 with $A = h(p), B = h(\tilde{p})$ and per-class Fano bounds in terms of $\delta_A^{(k)}, \delta_B^{(k)}$ and ϕ_{M_k} gives $I(h(p); h(\tilde{p})) \geq H(Y_k) - \phi_{M_k}(\delta_A^{(k)}) - \phi_{M_k}(\delta_B^{(k)})$. Since ϕ_{M_k} is non-decreasing on $[0, 1 - 1/M_k]$, replacing both errors by $\delta_h(Y_k) = \max(\delta_A^{(k)}, \delta_B^{(k)})$ only weakens the bound, giving $I(h(p); h(\tilde{p})) \geq H(Y_k) - 2\phi_{M_k}(\delta_h(Y_k))$. Taking the supremum over Y_k proves Eq. (15). The pass-only specialization replaces $\delta_h(Y_k)$ by the uniform upper bound $\delta_0 + \eta$ for all Y_k , again using monotonicity of ϕ_{M_k} (per-class).

The bound depends on the filter through δ_h , not on the curated choice of a single coarsening: it is the worst- Y_k Fano floor over a registered family of executable variables. This decouples the impossibility result from self-confirming variable selection. The Tri-Audit Protocol below reports the empirical δ_h for each Y_k , so the bound is observable rather than declarative.

Lemma 1 (Visible-spec entropy maximizer). *Fix a visible-example representation $V(p)$ on which the registered coarsenings act, and let \mathcal{Y}_V be the class of all measurable deterministic functions of $V(p)$ taking finitely many values up to M_V . Let $Y^{\text{full}} \in \mathcal{Y}_V$ be the canonical signature variable $V(p) \mapsto V(p)$ with M_V classes. Then for every $Y \in \mathcal{Y}_V$, $H(Y) \leq H(Y^{\text{full}})$, and equality holds when Y is a bijection of $V(p)$.*

Proof. Each $Y \in \mathcal{Y}_V$ is a deterministic function $Y = g(V(p))$, so by data processing $H(Y) \leq H(V(p)) = H(Y^{\text{full}})$.

To prevent self-favorable family selection, we adopt a two-step registration protocol: (i) the visible-example representation $V(p)$ is declared and frozen before any filter audit (output-type symbols plus output sign for up to three visible HumanEval doctests or MBPP assertions), and (ii) the registered family $\mathcal{Y}_{\text{exec}} \subseteq \mathcal{Y}_V$ must contain Y^{full} . Lemma 1 then implies that the $\sup_{Y_k} \{H(Y_k) - 2\phi_{M_k}(\delta_h(Y_k))\}$ in Eq. (15) is bounded below by the Y^{full} row, so an adversarial registrar cannot lower the formal floor by selecting only friendly coarsenings or by re-declaring $V(p)$ after seeing the filter. Coarser refinements ($Y^{\text{type}}, Y^{\text{sign}}$) trade $H(Y_k)$ for typically smaller δ_h , providing additional non-vacuous floor instantiations on rows where $\delta_h(Y^{\text{full}})$ approaches $1 - 1/M$.

Corollary 4 (Pass-Preserving Acceptance under Visible-Spec Registration). *Fix a registered family $\mathcal{Y}_{\text{exec}}$ satisfying the registration rule of Lemma 1. Suppose an acceptance rule for filter h is the conjunction of (i) hidden-test pass@1 movement $|\Delta_{\text{pass}_h}| \leq \eta$ and (ii) visible-spec preservation $\delta_h^{\max}(\mathcal{Y}_{\text{exec}}) \leq \delta_0 + \eta$. The role of the corollary is to make the covering relation explicit: pass@1 acceptance (i) does not on its own imply (ii) (Table 5 shows pass-preserving rows with $\delta_h^{\max} = 0.463$); pairing (i) with (ii) is therefore an operational extension of pass-only acceptance, and any acceptance rule that includes (ii) inherits the antecedent of Theorem 5. Then any h accepted under this rule satisfies*

$$I(h(p); h(\tilde{p})) \geq \mathcal{F}(\delta_0, \eta; \mathcal{Y}_{\text{exec}}), \quad (17)$$

where \mathcal{F} is the Fano floor of Eq. (16). On the HumanEval and MBPP registries this floor evaluates to $\mathcal{F}^{\text{op}} \geq 0.84$ and 1.20 nats at $(\delta_0, \eta) = (0.05, 0.05)$.

Proof. The deductive content uses (ii) only: condition (ii) is exactly the antecedent of Theorem 5, and the bound is then the floor of Eq. (16). The role of (i) is operational: it specifies the deployed acceptance rule that the corollary supplements with the visible-spec leg. The covering relation “(i) $\not\Rightarrow$ (ii)” is witnessed by Table 5 (pass-preserving rows with $\delta_h^{\max} = 0.463$). Numerical evaluation of \mathcal{F}^{op} uses the registry-rule recomputation in the supplement.

Corollary 4 formalizes the role of visible-spec registration as the bridge between hidden-test pass@1 acceptance and the Fano floor: the impossibility statement does not require pass@1 alone to imply $\delta_h^{\max} \leq \delta_0 + \eta$, but it does show that any acceptance rule that pairs pass@1 with mandatory visible-spec registration inherits the same quantitative

residue \mathcal{F} . Filters whose acceptance rule omits the visible-spec leg fall outside the theorem’s scope and are reported as registered-family collapse in the empirical Tri-Audit; this is the covering relation that makes the theorem applicable to deployed pass@1-style acceptance rules while keeping its antecedent precise.

Corollary 5 (Dataset-Agnostic Visible-Spec Floor). *Let \mathcal{D} be any benchmark whose canonical solutions induce a visible-spec representation $V(p)$ on the prompt with M_V classes and prompt-distribution entropy $H(V(p))$. Let $\mathcal{Y}_{\text{exec}} \subseteq \mathcal{Y}_V$ contain Y^{full} (registration rule of Lemma 1). Then for any deterministic filter h accepted under Corollary 4’s pass@1 + $\delta_h^{\text{max}} \leq \delta_0 + \eta$ rule,*

$$I(h(p); h(\tilde{p})) \geq H(V(p)) - 2\phi_{M_V}(\delta_0 + \eta). \quad (18)$$

The right-hand side is non-trivial whenever $H(V(p)) > 2\phi_{M_V}(\delta_0 + \eta)$, equivalently whenever the visible-spec distribution carries more than $2\phi_{M_V}(\delta_0 + \eta)$ nats of benchmark-conditional entropy.

Proof. Apply Theorem 5 on the registered family that contains Y^{full} , then use Lemma 1 to lower bound the supremum by the Y^{full} row.

Corollary 5 states the residue purely as a function of the visible-spec entropy $H(V(p))$ and the registered cardinality M_V , with no reference to a specific benchmark. This yields a robustness statement under *any* prompt-side transformation that preserves $V(p)$ and M_V : hidden-test expansion, prompt re-tokenization, syntax-level canonicalization that preserves the visible doctest signature, and any other manipulation that leaves the registered visible-spec parse bit-equal. Two benchmarks instantiate the floor on disjoint visible-spec representations: HumanEval registers $H(V(p)) = 2.19$ nats with $M_V = 34$ and $\phi_{34}(0.10) \leq 0.675$ nats; MBPP registers $H(V(p)) = 2.17$ nats with $M_V = 21$ and $\phi_{21}(0.074) \leq 0.486$ nats. *Hidden-test extension invariance* on EvalPlus is then a direct empirical witness of this robustness, and a parser-stability check on our $V(p)$ pipeline: the F1 visible-spec parser reports bit-equal signature sequences on 164/164 (100%) HumanEval+ prompts and 224/224 (100%) MBPP+ prompts matched on the original task ids (supplementary material), so by Corollary 5 the matched-subset floors satisfy $\mathcal{F}^{\text{op,HE+}} = \mathcal{F}^{\text{op,HE}}$ and $\mathcal{F}^{\text{op,MB+}} = \mathcal{F}^{\text{op,MB}}$. We do not present EvalPlus as a third independent benchmark instantiation; we present it as the test that the dataset-agnostic form survives the canonical pass@1-strengthening route of expanding hidden test suites and as the test that the F1 visible-spec parser is stable under the EvalPlus prompt pipeline. The bound degrades gracefully on benchmarks with low visible-spec entropy (e.g. a dataset whose docstring expected outputs are dominated by a single Boolean return type), where it correctly reports a small \mathcal{F}^{op} : the impossibility statement is then weaker because the public visible-spec channel is genuinely lower-entropy, not because the result is benchmark-specific.

Numerical floor on HumanEval and MBPP. We register a non-singleton family $\mathcal{Y}_{\text{exec}}^{\text{HE}} = \{Y_{\text{HE}}^{\text{full}}, Y_{\text{HE}}^{\text{type}}, Y_{\text{HE}}^{\text{sign}}\}$ on MBPP,

where Y^{full} is the output-signature vector parsed from up to three visible executable examples, Y^{type} retains output type only, and Y^{sign} retains the sign of numeric outputs only. All three coarsenings are deterministic functions of the visible examples, so Theorem 5 applies row-wise; we report the worst- Y_k floor in Table 3 and prose. The headline Y^{full} row gives $M = 34$, $H(Y_{\text{HE}}^{\text{full}}) = 2.19$ nats and $M = 21$, $H(Y_{\text{MB}}^{\text{full}}) = 2.17$ nats; the type-only and sign-only coarsenings have strictly fewer classes and lower $H(Y_k)$, so Y^{full} is the floor maximizer.

The Fano floor admits two strictly-positive instantiations that we report separately. The *formal pass-only floor* substitutes the uniform upper bound $\delta_0 + \eta$ for $\delta_h(Y_k)$ in Eq. (16): with near-identity baseline $\delta_0 \leq 0.05$ on HumanEval and $\delta_0 \leq 0.024$ on MBPP, a pass-only rule at $\eta = 0.05$ leaves $\mathcal{F}_{\text{HE}}^{\text{op}} = 2.19 - 2\phi_{34}(0.10) \geq 0.84$ nats and $\mathcal{F}_{\text{MB}}^{\text{op}} = 2.17 - 2\phi_{21}(0.074) \geq 1.20$ nats. This is the formal impossibility number: any pass-preserving filter that the acceptance rule can certify must leave at least this much shared filtered-prompt channel.

The *identity-row realized Fano lower bound* substitutes the per-row empirical $\delta_A^{(k)}, \delta_B^{(k)}: \mathcal{F}_{h_{\text{id,HE}}}^{\text{id}} \geq 1.67$ nats and $\mathcal{F}_{h_{\text{id,MB}}}^{\text{id}} \geq 1.80$ nats on the identity filter (Table 3). This realized bound is above the formal pass-only floor because the identity filter’s realized decoder error is well below $\delta_0 + \eta$, but it is a row-wise realization on a single h , not a tighter universal floor. Together the two quantities give a layered impossibility: the formal floor \mathcal{F}^{op} proves a non-trivial lower bound for every pass-only-accepted filter, and the identity-row realization demonstrates tightness for the identity row used as the audit anchor. Both floors are reported on the same Shannon-nats scale used by the Tri-Audit gate (§6).

Corollary 6 (Estimator-Invariant No-Certificate). *Let E be any deterministic measurable embedding such that $H(C | E(h(p))) \leq \epsilon_A^E$ and $H(C | E(h(\tilde{p}))) \leq \epsilon_B^E$. Then*

$$I(E(h(p)); E(h(\tilde{p}))) \geq H(C) - \epsilon_A^E - \epsilon_B^E. \quad (19)$$

In particular, applying E to a filtered prompt before estimating mutual information cannot lower the no-certificate floor below $H(C) - \epsilon_A^E - \epsilon_B^E$. Whenever E preserves the executable- equivalence variable Y in the Fano sense of Corollary 3, the floor is at least $H(Y) - \phi_M(\delta_A^E) - \phi_M(\delta_B^E)$.

Proof. Theorem 3 applied to $(E(h(p)), E(h(\tilde{p})), C)$ gives the entropy-submodularity lower bound; substituting the two conditional-entropy bounds proves Eq. (19). The Fano specialization repeats the proof of Corollary 3 on $(E(h(p)), E(h(\tilde{p})), Y)$.

The corollary makes the no-certificate conclusion estimator-invariant: any deterministic embedding pipeline used by an MI estimator inherits the same shared-channel floor whenever the embedding does not destroy task information. Empirical estimator-family checks therefore probe finite-sample behavior of the same population inequality, not separate audit objects.

4 Experimental Setup

Models. The primary slate $\mathcal{S}^{\text{prim}}$ comprises CodeLlama-7B-Instruct (Rozière et al. 2023), Qwen2.5-Coder-7B-Instruct (Hui et al. 2024), DeepSeek-Coder-6.7B-Instruct (Guo et al. 2024), and Qwen2.5-Coder-1.5B-Instruct (Hui et al. 2024), all quantized to INT4 (NF4) for fitting on a single 24GB GPU and evaluated at $n = 164$. The primary slate spans three distinct pretraining families (Llama-derivative, Qwen2.5-Coder, DeepSeek-Coder), with the Qwen2.5-Coder family represented at two scales (7B and 1.5B), three distinct instruction-tuning recipes, and a $4.7\times$ scale ratio between the smallest and largest backbone. A supplementary cross-architecture probe $\mathcal{S}^{\text{supp}} = \{\text{StarCoder2-7B-Instruct}\}$ (Lozhkov et al. 2024), INT4 (NF4), $n = 50$ subset, additionally tests a non-Llama transformer architecture (StarCoder2 attention and tokenizer); it is reported alongside but not part of the primary cross-model invariance claim.

Datasets. HumanEval (164 problems, function-completion benchmark (Chen et al. 2021)). Cell H replicates the bound on MBPP-sanitized (257 hand-curated programming problems (Austin et al. 2021); first $n = 164$ used to match HumanEval sample size), and the executable-equivalence bridge uses HumanEval visible doctests together with MBPP visible assertions. We additionally attempted SecurityEval (121 CWE-tagged problems (Siddiq and Santos 2022)), but its schema is incompatible with output-only function-body extraction; we document this as a schema caveat in the supplementary material rather than a main diagnostic cell.

Embedding extraction (output-only). Theorem 1 treats c_π and \tilde{c}_π as random variables over token sequences; Corollary 1 gives the corresponding bound for any deterministic embedding of those sequences. To estimate $\text{Sec} = \text{I}(z_\pi; \tilde{z}_\pi)$ in the embedding domain without breaking the underlying Markov chain $z_\pi \rightarrow p \rightarrow \tilde{p} \rightarrow \tilde{z}_\pi$, the embedding map must be a function of the generation alone, not of the prompt-generation joint state. We feed each generated function body *by itself* (without the originating prompt) through a fresh forward pass and extract the last-token hidden state of the final transformer layer; PCA reduction to $d = 8$ before MI estimation. This variable design is the one required by step (ii) of the proof. Cell D ablates the pooling (mean over body tokens) and cell E the PCA dimension ($d = 16$). Table 1 separates this theorem-bound protocol from the context-mixed cosine used only for per-problem correlation and from the prompt-side leakage estimate used in the RHS budget.

The embedded experiments are estimator-level diagnostics of Corollary 1, not sequence-level measurements of Theorem 1. After PCA, z^* , z_π , and \tilde{z}_π are continuous hidden-state variables, so the reported $\text{H}(z^*)$, Cap , and Sec are differential-entropy / neural-MI proxy values tied to the fixed embedding, preprocessing, and MI-estimator pipeline. They are not empirical Shannon entropies over the finite set of benchmark indices and therefore are not bounded by $\log n$. We interpret residuals and saturation only within that pipeline, not as absolute sequence-level information val-

ues or as quantities comparable across incompatible embeddings.

Table 1: Embedding protocols used for distinct quantities. Only the output-only generation embedding enters the embedded diagnostic check; the context-mixed cosine is a separate per-problem signal.

Quantity	Embedding input	Role
$\text{Sec} = \text{I}(z_\pi; \tilde{z}_\pi)$	generated code only	embedded diagnostic MI
alignment-pass@1 signal	prompt code	per-problem correlation
$\text{I}(p; \tilde{p})$	prompt only	RHS leakage proxy

The RHS proxy ledger is as follows. Table 2 uses the original-prompt PCA/MINE proxy $\hat{I}_{\text{prompt}}(p, \tilde{p})$ with maximum 12.58 nats from Table 20. Table 4 recomputes a separate filtered-prompt proxy $\hat{I}_{\text{prompt}}(h(p), h(\tilde{p}))$ for each model/filter. Neither quantity is the output-only generation-retention proxy $\widehat{\text{Sec}}$, and neither is the context-mixed cosine used for per-problem alignment.

Mutual information estimators. MINE (Belghazi et al. 2018) with 500 training steps, batch over the entire n problems. KNN-based KSG estimator (Kraskov, Stögbauer, and Grassberger 2004) at $k = 3$ as a comparison.

Perturbation pool. We use five prompt perturbation families: (i) *synonym*, replacing instruction verbs (Check \rightarrow Verify); (ii) *negation*, inserting a “be lenient” caveat; (iii) *comment*, appending performance or input-validation comments; (iv) *security-anti*, appending comments that disable security checks; (v) *identifier*, renaming variables (numbers \rightarrow x, threshold \rightarrow thr). In the 23-pool search, the comment row includes security-directed comment variants; Table 20 reports the prompt-side leakage of the security-anti family separately.

5 Embedded Diagnostic Check for the Cap-Sec Decomposition

5.1 Main Bound Table

We test estimator-level consistency of the embedded-variable bound across seven configurations under the stated PCA/MINE protocol. For each row we report

$$\begin{aligned} \text{RHS}_{\text{emb}} &:= \text{H}(z^*) + \max_T \text{I}(p; \tilde{p}), \\ \text{Residual} &:= \text{RHS}_{\text{emb}} - (\text{Cap} + \max_T \text{Sec}), \\ \text{Saturation} &:= \frac{\text{Cap} + \max_T \text{Sec}}{\text{RHS}_{\text{emb}}}. \end{aligned} \quad (20)$$

A positive residual under MINE is an estimator sanity check, not certified sequence-level slack or evidence that the population boundary is achievable.

The table reports $\text{H}(z^*)$ for the embedded canonical solution $z^* = E(c^*)$, not the sequence-level entropy $\text{H}(c^*)$ from Theorem 1. Three main runs (F, G, H) at full $n = 164$ span two models (CodeLlama-7B, Qwen2.5-Coder-7B) and two

Table 2: Estimator-level consistency check for the embedded Capacity-Security diagnostic under the output-only embedding protocol. The table reports the embedded-variable proxy from Corollary 1 with $z^* = E(c^*)$, $z_\pi = E(c_\pi)$, $\tilde{z}_\pi = E(\tilde{c}_\pi)$. The RHS, residual, and saturation are defined in Eq. (20); saturation is interpreted only within the same embedding/PKA/MI-estimator pipeline. Cell letters are protocol identifiers fixed at letter-assignment time; cell B is a reserved letter never instantiated and cell C (SecurityEval) is in the supplement. Cell A reports mean (std) over three $n = 50$ seeds; its mean includes one estimator-stressed seed (§9). HE: HumanEval; MBPP: MBPP-sanitized; lt/mp: last-token / mean-pool; I4: INT4 NF4. All seven cells are numerically inside the embedded diagnostic region.

Cell	Cfg.	n	Cap	$\min_T \text{Sec}$	$\max_T \text{Sec}$	$H(z^*)$	RHS	resid.	sat.
A (3 seeds)	HE/CL/lt8/I4	50	3.02 (.69)	6.51 (1.07)	21.0 (4.5)	14.9 (0.7)	27.5 (0.7)	3.40 (4.5)	0.87 (.17)
D	HE/CL/mp8/I4	50	5.43	8.68	23.50	18.71	31.28	2.36	0.92
E	HE/CL/lt16/I4	50	3.81	8.42	25.26	30.29	42.87	13.80	0.68
F	HE/CL/lt8/I4	164	1.68	4.83	13.70	12.84	25.42	10.04	0.61
G	HE/Qw/lt8/I4	164	2.27	5.01	7.61	24.24	36.82	26.94	0.27
H	MBPP/CL/lt8/I4	164	2.09	5.74	15.23	14.09	26.67	9.35	0.65
I	HE/CL/lt8/BF16	50	2.90	6.16	17.49	16.84	29.42	9.03	0.69

datasets (HumanEval, MBPP-sanitized). Three estimator ablations (D mean-pool, E PCA-16, I BF16) test embedding pooling, projection dimension, and weight precision. Cell A reports the mean \pm std of three random seeds at $n = 50$ HumanEval to characterize MINE noise. Across the six individual rows, the embedded check has saturation between 0.27 and 0.92 and estimator residuals from 2.36 to 26.94 nats. The three-seed stability row has mean saturation 0.87 and mean residual 3.40 nats, with one MINE-stressed seed audited in §9. SecurityEval (cell C) appears in the supplementary material as a schema caveat: its canonical-solution schema lacks an entry-point name, and reference extraction degrades. The bound direction still passes there (slack +4.14 nats), but the saturation ratio is not meaningful because $H(z^*)$ degenerates under the schema mismatch. We exclude it from the main table to keep the protocol uniform.

5.2 Stability Across Seeds (Cell A)

Three random shuffles of HumanEval at $n = 50$ give $\text{Cap} = 3.02 \pm 0.69$, $\min_T \text{Sec} = 6.51 \pm 1.07$, $\max_T \text{Sec} = 21.04 \pm 4.47$, and estimator residual 3.40 ± 4.47 nats on average; two seeds have positive residual and the third reaches saturation 1.01 under MINE, which we audit as estimator stress in §9. The Sec-Cap margin $\min_T \text{Sec} - \text{Cap}$ remains positive in all three seeds.

5.3 Full-precision audit (BF16, Cell I)

To check quantization, we re-run the cell-F protocol on CodeLlama-7B at BF16 full precision with $n = 50$. We obtain $\text{Cap} = 2.90$, $\min_T \text{Sec} = 6.16$, $\max_T \text{Sec} = 17.49$, theorem residual 9.03 nats, saturation 0.69, and pass@1 46% (vs. 36% at INT4). The embedded diagnostic is precision-stable in this regime: precision changes Cap and Sec proportionally, while residual and saturation stay in the INT4 range. A context-mixed embedding protocol (forwarding $p \parallel c$ rather than c alone) would conflate prompt-context information with the generation, inflate Cap-Sec correlation, and produce artificially small residual at BF16. The output-only protocol separates these quantities.

5.4 Cross-Dataset Replication on MBPP (Cell H)

Cell H repeats the cell-F protocol on MBPP-sanitized (Austin et al. 2021) with $n = 164$. We obtain $\text{Cap} = 2.09$, $\min_T \text{Sec} = 5.74$, $H(z^*) = 14.09$, $\text{Sec-Cap margin} + 3.65$ nats, saturation 0.65, and estimator residual 9.35 nats. Pass@1 is 47.6% (vs. 36.0% on HumanEval). Under the separate context-mixed per-problem protocol used in §7, the alignment cosine also correlates with pass@1 on MBPP (Spearman $\rho = 0.225$, $p = 0.0038$). The DeepSeek-Coder Tri-Audit also replicates on MBPP at $n = 164$ (identity pass@1 0.646, $\hat{\text{I}}_{\max} = 20.17$, $\hat{\text{S}}_{\text{ec}\max} = 13.89$): all four pass-preserving deterministic rows (strip_comments, normalize_template, combined, first_sentence_docstring) Tri-fail, remove_examples loses pass@1 by 7.9 points (capacity-loss boundary), and signature_only is a capacity-loss control. Thus both the output-only embedded diagnostic and the prompt-conditioned alignment signal replicate on a curated benchmark with a different problem mix, and the Tri-Audit Invariance survives the cross-dataset jump.

6 Leakage-Guided Prompt Hardening

Definition 3 (Tri-Audit Protocol). A *Tri-Audit* for a candidate prompt filter h on a model π , a perturbation pool \mathcal{T} , and a registered coarsening family $\mathcal{Y}_{\text{exec}}$ tests three objectives under the same fixed estimator pipeline relative to the identity filter: (1) task preservation, (2) filtered prompt-channel reduction, and (3) clean-perturbed output-retention non-increase. The task-preservation objective uses two complementary screens that together match the antecedent of Theorem 5: (1a) clean pass@1 movement Δ_{pass_h} , and (1b) visible-spec preservation $\delta_h^{\max}(\mathcal{Y}_{\text{exec}}) := \sup_{Y_k} \max(\delta_A^{(k)}, \delta_B^{(k)})$. The leakage and retention objectives are reported on two axes. The *prompt-side deductive axis* uses the Fano-derived in-family lower bound $\hat{\text{I}}_h^{\text{b}}(Y_k) := H(Y_k) - \phi_{M_k}(\delta_A^{(k)}) - \phi_{M_k}(\delta_B^{(k)})$ on the registered family $\mathcal{Y}_{\text{exec}}$, which lives on the same Shannon-nats scale as \mathcal{F}^{op} and \mathcal{F}^{id} . The prompt-side axis is a deductive registry attribute: by Theorem 5, any antecedent-preserving filter satisfies $\hat{\text{I}}_h^{\text{b}}(Y^{\text{full}}) \geq \mathcal{F}^{\text{op}}$ automatically; we therefore report the

prompt-side axis once per (filter, dataset) registry row rather than per backbone, and treat it as a deductive registry attribute documenting the inherited prompt-side residue rather than an empirical gate. The *model-side empirical proxy axis* uses the fixed-estimator MINE/KSG-on-PCA quantities $\Delta\widehat{I}_h := \max_{T \in \mathcal{T}} \widehat{I}(h(p); h(\tilde{p})) - \max_{T \in \mathcal{T}} \widehat{I}(p; \tilde{p})$ and $\Delta\widehat{\text{Sec}}_h := \max_{T \in \mathcal{T}} \widehat{\text{Sec}}_h - \max_{T \in \mathcal{T}} \widehat{\text{Sec}}$ on a deterministic embedding pipeline (§9); the model-side axis is genuinely backbone-dependent and carries the empirical content of the audit. The two axes are unit-consistent within themselves and not directly comparable across. A filter *Tri-passes* under tolerances (η, ρ) when all four conditions hold: $\Delta\text{pass}_h \geq -\eta$ (pass@1 movement), $\delta_h^{\max}(\mathcal{Y}_{\text{exec}}) \leq \delta_0 + \eta$ (visible-spec antecedent), $\Delta\widehat{I}_h/\widehat{I} \leq -\rho$ (proxy leakage reduction), and $\Delta\widehat{\text{Sec}}_h \leq 0$ (retention non-increase). The default operating point is $(\eta, \rho) = (5 \text{ pts}, 0.25)$. The *Tri-Audit* name reflects the three objectives (1)–(3); the four conditions instantiate them by realizing objective (1) through the two complementary screens (1a) and (1b) that together match the antecedent of Theorem 5, with (2) and (3) discharged empirically on the model-side proxy axis, so the protocol still tests three objectives even though it gates four conditions. The prompt-side deductive registry attribute is reported alongside as a documentation of the floor inherited by every antecedent-preserving filter; it is not a fifth empirical gate. The visible-spec preservation screen $\delta_h^{\max} \leq \delta_0 + \eta$ is the operational realization of Theorem 5’s antecedent on the registered family $\mathcal{Y}_{\text{exec}}$, not an additional empirical leg: filters that violate this screen lie outside the theorem’s scope and are reported as *registered-family collapse* rather than as *Tri-pass* candidates. Pass@1 alone does not imply $\delta_h^{\max} \leq \delta_0 + \eta$ (e.g. Table 3 reports $\delta_h(Y^{\text{full}}) = 0.463$ for the example-removal row at only 1.8 clean-pass points lost), so the screen has to be checked separately. The adversarial visible-spec-corruption filter family (doctest-corrupt attack, strong doctest-corrupt attack, Table 9) is a registered-family collapse attack: it preserves prompt narrative, signature, and >>> call lines but replaces each docstring expected-output token, so δ_h^{\max} on $\mathcal{Y}_{\text{exec}}$ jumps to ≥ 0.5 by construction. On Qwen-1.5B both attack rows satisfy the three measurement legs (clean pass drop $\leq 5\text{pt}$, $\Delta\widehat{I}/\widehat{I} = -26.8\%$ and -27.2% , $\Delta\widehat{\text{Sec}} \leq 0$); the visible-spec antecedent rejects them as registered-family collapse, demonstrating that the antecedent is operationally non-vacuous and that pass@1 plus the proxy gate alone would otherwise admit visible-spec-collapsing filters. The *Fano-anchored* reading of the prompt-side axis reads ρ^* from the bound on the same Shannon-nats scale that defines \mathcal{F} . Let $\widehat{I}_{\text{id}}^{\text{b}}(Y_k) := H(Y_k) - \phi_{M_k}(\delta_A^{(k), \text{id}}) - \phi_{M_k}(\delta_B^{(k), \text{id}})$ be the Fano-derived lower bound on $I(p; \tilde{p})$ for the identity filter under coarsening $Y_k \in \mathcal{Y}_{\text{exec}}$; both \mathcal{F} and $\widehat{I}_{\text{id}}^{\text{b}}$ are pure Shannon-nats quantities extracted from the same visible-spec decoder. The Fano-anchored relation

$$\widehat{I}_{\text{id}}^{\text{b}}(Y_k) - \widehat{I}_h^{\text{b}}(Y_k) \geq \widehat{I}_{\text{id}}^{\text{b}}(Y_k) - \mathcal{F}(\delta_0, \eta; \mathcal{Y}_{\text{exec}}), \quad (21)$$

holds automatically on every antecedent-preserving filter as a deductive consequence of Theorem 5; we therefore record

it as a prompt-side registry attribute rather than as an empirical gate. Definition 3’s $(\eta, \rho) = (5 \text{ pts}, 0.25)$ is the empirical operating point on the model-side proxy axis used in the experiments.

The Tri-Audit Protocol is the operational instantiation of Theorem 4 and Corollary 6: a pass-only acceptance rule is the special case in which only Δpass_h is checked, and the no-certificate floor implies that this restriction admits filters with non-trivial residual prompt-channel and retention movement. Reporting all three quantities turns hardening evaluation from a pass/fail report into a vector verdict that other authors can audit and challenge.

Proposition 1 (Tri-Audit Failure-Mode Coverage in \mathcal{H}). *Each of the four Tri-Audit conditions of Definition 3 is binding on the audited family \mathcal{H} : there exists at least one row in \mathcal{H} whose rejection is decided by the listed condition. The audit identifies four mutually distinguishable failure modes: a capacity-loss row whose primary failure is C_1 ; a registered-family-collapse row whose primary failure is C_2 ; a trivial filter whose primary failure is C_3 ; and a Pareto-degenerate retention-inflation row whose primary failure is C_4 . Rows may violate more than one condition simultaneously; the proposition’s content is the existence of four mutually distinguishable failure-mode equivalence classes on the audited primary slate, not the construction of single-condition witnesses.*

Proof by enumeration of audited rows. We list one representative row per failure mode and indicate which condition is the informative one for the rejection.

(i) *Capacity-loss mode* (primary failure C_1). The signature-only filter row on CodeLlama (Table 6) has $\Delta\text{pass}_h = -13.4 \text{ pts}$, $\Delta\widehat{I}/\widehat{I} = -41.1\%$, $\Delta\widehat{\text{Sec}} = -5.6 \text{ nats}$; the row is rejected because pass@1 collapses beyond η , which is the operational definition of capacity loss for a hardening rule. (The same row also fails C_2 on the registered $\mathcal{Y}_{\text{exec}}$ with $\delta_h^{\max} = 0.280$, but the deployment-relevant information for a practitioner reading this row is the pass-drop magnitude and the resulting capacity loss, not the visible-spec antecedent.)

(ii) *Registered-family-collapse mode* (primary failure C_2). The doctest-corrupt attack adversarial attack family on Qwen-Coder-1.5B (Table 9) has $\Delta\text{pass}_h \in [-1.8, 0]$, $\Delta\widehat{I}/\widehat{I} = -26.8\%$ and -27.2% , $\Delta\widehat{\text{Sec}} \leq 0$, and $\delta_h^{\max} \geq 0.5$. The remaining three conditions are all satisfied at the audited operating point, so the informative rejection is the visible-spec antecedent: dropping C_2 admits a filter that preserves pass@1 and reduces the proxy leakage while collapsing $V(p)$ on which the floor is defined.

(iii) *Trivial-filter mode* (primary failure C_3). The identity filter h_{id} trivially passes C_1, C_2, C_4 but has zero proxy-leakage reduction by definition. Dropping C_3 admits the identity as a hardening certification, which is vacuous; the informative rejection is the requirement for non-trivial proxy reduction.

(iv) *Pareto-degenerate retention-inflation mode* (primary failure C_4). The Qwen-7B preserve canon. learned-canonicalizer row on Qwen-Coder-7B (Table 5) has

$\Delta_{\text{pass}_h} = 0.0$ pts, $\widehat{\Delta I} = -2.15$ nats (the only audited row with negative leakage proxy at zero pass drop), and $\widehat{\Delta \text{Sec}} = +0.87$ nats. The row’s proxy-leakage reduction is -12% , so it does not clear the headline -25% leakage gate either; however, the informative deployment signal is the retention inflation $\Delta \widehat{\text{Sec}} > 0$, which an unrestricted weakening of the audit to “leakage proxy negative regardless of magnitude” would otherwise admit. The audit’s C_4 leg is therefore independently load-bearing: a row that moves leakage and retention in opposite directions on the proxy axis is a Pareto-degenerate hardening attempt that the Cap-Sec ledger of Theorem 3 explicitly accounts for.

Reading the audit-coverage result. Drop any one of the four Tri-Audit conditions and Proposition 1 identifies a registered row that the audit would then admit despite no practitioner calling it hardening (capacity loss, registered-family collapse, identity, or Pareto-degenerate retention inflation). The empirical Cross-Model Tri-Audit Invariance is therefore not over-specified at the coverage level. A stronger minimality claim, that each condition can be isolated by a witness violating only that condition, would require augmenting \mathcal{H} with rows tracing the four corners of the condition hypercube; we leave this construction to the pre-registered extension harness in the supplementary material.

Theorem 3 and Corollary 2 turn prompt hardening into a Pareto audit. A useful filter must preserve task capacity while reducing the filtered prompt channel and the clean-perturbed retention channel. A filter that preserves execution accuracy can still leave the perturbation channel open; a filter that suppresses the channel can also remove task information needed for generation. We therefore evaluate prompt hardening by three quantities at once: clean pass@1, prompt leakage $I(h(p); h(\hat{p}))$, and clean-perturbed retention Sec_h . Pass@1 is used as an operational capacity proxy, not as a direct estimator of the conditional entropy terms in Theorem 3; preserving pass@1 is necessary evidence that a filter has not destroyed the task, but it is not sufficient evidence that $H(C | h(p))$ is small.

We test deterministic filters that require no model training and no access to generated code: comment stripping, template normalization, example-block removal, first-sentence docstring retention, their composition, and a signature-only negative control. These filters span the frontier from near-identity transforms to aggressive prompt compression. The signature-only filter is a hard capacity-loss control: it strips prompt content and is not expected to preserve task performance. The filters are applied symmetrically to clean and perturbed prompts before generation. We use the same output-only embedding protocol as the bound table for Sec_h , and a prompt-only PCA/MINE estimate for the filtered leakage term. Table 4 reports the resulting budget utilization

$$U_h = \frac{\text{Cap}_h + \max_T \text{Sec}_h}{H(z^*) + \max_T I(h(p); h(\hat{p}))}. \quad (22)$$

The executable-equivalence cell is the positive bridge from the theorem to executable specifications. It instantiates Corollary 3 on a finite visible-spec variable Y parsed from HumanEval doctests and MBPP assertions, coarsened

by output type and sign. For HumanEval, near-identity filters retain $M = 34$ visible-spec classes with $H(Y) = 2.19$ nats and Fano lower bounds of 1.67–1.71 nats. MBPP gives a second visible-spec check with $M = 21$, $H(Y) = 2.17$ nats, and a 1.80-nat near-identity lower bound. Rows that preserve examples keep small Fano terms; rows that remove examples or reduce the prompt to a signature-only stub collapse the lower bound. This cell shows that the task-preservation lower bound can be made observable for finite executable specifications; the broader pass@1 frontier below tests the same audit principle under the declared leakage/retention proxies.

The hardening cell is not a claim that deterministic filtering solves prompt robustness. It is a Pareto audit motivated by Theorem 3: task-preserving filters should be expected to retain shared clean-perturbed information unless they discard task capacity. This also means that total filtered-prompt MI is a conservative total-channel diagnostic: it intentionally captures both benign task semantics and perturbation-specific residue. The residual perturbation-leakage cell in Table 7 resolves this confound rather than discarding the total-channel signal. A task-blocked classifier predicts the perturbation family from $E(h(\hat{p})) - E(h(p))$, so the clean filtered task representation is subtracted before the residual is tested. This makes perturbation identity recoverability observable after controlling for task-preserving shared information.

The residual audit shows that the proxy is not merely rewarding prompt compression, and the split-level result is stable. On CodeLlama-7B hidden-state prompt embeddings, identity prompts retain a strong perturbation-family signal (balanced accuracy 0.790 with empirical 95% interval [0.744, 0.836], versus permutation 0.250). Comment stripping reduces this signal by 50.8% [46.3, 56.0], the combined deterministic filter by 59.9% [56.1, 63.7], Qwen-7B preserve canonicalization by 60.5% [54.6, 66.5], and Qwen-1.5B minimal canonicalization by 60.6% [56.2, 64.3]. In contrast, template normalization and example removal preserve pass@1 but leave residual perturbation predictability unchanged: their reduction intervals include zero (-0.5% [$-7.0, 3.8$] and -1.1% [$-6.0, 5.2$]). The signature-only negative control also reduces residual leakage but loses capacity, which keeps the Pareto tradeoff visible.

The fixed-proxy audit policy turns the theorem into a reproducible decision rule: a row must preserve pass@1 while showing leakage-proxy reduction and no retention increase under the same declared estimator pipeline. Table 8 combines the residual audit with the original total-channel and retention gate. It exposes two complementary failure modes. Combined filtering and learned canonicalizers remove perturbation identity but remain residual-only because total-channel leakage or output retention does not also decrease. Example removal reduces the old total-channel and retention proxies but leaves perturbation identity recoverable. Signature-only filtering removes residue by losing task capacity. Thus the residual audit strengthens, rather than replaces, the full Pareto gate.

Table 6 groups the same filters by design intent. A pass-only evaluation would accept the near-identity sanitizer and

Table 3: Visible-spec executable-equivalence positive control for Corollary 3. The finite task variable Y is an output-signature vector computed from up to 3 visible executable examples: HumanEval doctests and MBPP assertions. The decoder sees only the filtered prompt $h(p)$ or $h(\tilde{p})$ and parses retained visible examples. Rows that preserve executable examples have small Fano terms; rows that remove or truncate examples become capacity-loss controls for this finite executable-specification variable. The lower bound is $H(Y) - \phi_M(\delta_A) - \phi_M(\delta_B)$ using the worst audited perturbation for δ_B . This table demonstrates observability of the finite-variable lower bound; it does not support hidden-test pass@1 claims.

Dataset	filter	M	$H(Y)$	clean err.	worst pert. err.	worst T	lower bound
HumanEval	none	34	2.19	3.0	3.7	comment	1.67
HumanEval	strip comments	34	2.19	3.0	3.0	synonym	1.71
HumanEval	normalize template	34	2.19	3.0	3.7	comment	1.67
HumanEval	combined	34	2.19	3.0	3.0	synonym	1.71
HumanEval	remove examples	34	2.19	46.3	46.3	synonym	0.00
HumanEval	first sentence	34	2.19	43.9	43.9	synonym	0.00
HumanEval	signature only	34	2.19	28.0	28.0	synonym	0.00
MBPP	none	21	2.17	2.4	2.4	synonym	1.80
MBPP	strip comments	21	2.17	2.4	2.4	synonym	1.80
MBPP	normalize template	21	2.17	2.4	2.4	synonym	1.80
MBPP	combined	21	2.17	2.4	2.4	synonym	1.80
MBPP	remove examples	21	2.17	100.0	100.0	synonym	0.00
MBPP	first sentence	21	2.17	2.4	2.4	synonym	1.80
MBPP	signature only	21	2.17	100.0	100.0	synonym	0.00

Table 4: Empirical Pareto audit of deterministic prompt hardening on HumanEval. A prompt filter h is applied before generation to both clean and perturbed prompts. We report clean pass@1, mean perturbed pass@1 across audited perturbation classes, the largest measured embedded prompt-leakage proxy $\max_T \widehat{I}(h(p); h(\tilde{p}))$, the largest output-retention proxy $\max_T \widehat{Sec}_h$, and budget utilization $U_h = (\widehat{Cap}_h + \max_T \widehat{Sec}_h) / (\widehat{H}(z^*) + \max_T \widehat{I}(h(p); h(\tilde{p})))$. Values are comparable within the fixed model/filter embedding and MINE pipeline; increases across filters are diagnostic failures, not violations of raw prompt-variable DPI. proxy pass under this fixed pipeline requires at least 25% leakage-proxy reduction relative to the identity filter, clean pass@1 loss no more than 5 absolute points, and no increase in $\max_T \widehat{Sec}_h$; the 25% rule is an audit policy rather than an estimator-certified safety threshold. Signature only is a negative control for capacity loss.

Model	Filter h	n	clean	pert.	$\max \widehat{I}_h$	$\max \widehat{Sec}_h$	U_h	verdict
CodeLlama	none	164	36	33	12.35	12.98	0.58	baseline
CodeLlama	strip comments	164	36	35	18.33	18.04	0.63	weak
CodeLlama	normalize template	164	36	33	13.75	13.16	0.56	weak
CodeLlama	remove examples	164	34	33	11.45	12.15	0.55	weak
CodeLlama	first sentence	164	30	29	14.53	18.27	0.70	weak
CodeLlama	combined	164	36	35	18.79	14.66	0.52	weak
CodeLlama	signature only	164	23	22	17.42	13.71	0.49	capacity loss
Qwen	none	164	84	82	18.59	8.27	0.25	baseline
Qwen	strip comments	164	84	83	29.82	10.36	0.24	weak
Qwen	normalize template	164	83	82	22.04	7.83	0.22	weak
Qwen	remove examples	164	81	80	19.24	8.04	0.24	weak
Qwen	first sentence	164	50	49	19.19	7.23	0.22	capacity loss
Qwen	combined	164	83	82	31.70	8.89	0.20	weak
Qwen	signature only	164	31	31	18.21	8.60	0.26	capacity loss

Table 5: Constrained best-of-family search over audited prompt filters under the two-axis reporting protocol (Definition 3). Rows are the audited filters that satisfy the declared task-collapse constraint: clean pass@1 loss is at most 5 absolute points relative to the identity filter on the same model. The *prompt-side deductive column* $\widehat{I}_h^{\text{lb}}(Y^{\text{full}})$ is the Fano-derived in-family lower bound on $I(h(p); h(\widehat{p}))$ in Shannon nats, computed prompt-side from the visible-spec decoder errors of Table 3; this column is a registry attribute of (h, V) that is backbone-invariant by construction and is reproduced across the four primary backbones and the StarCoder2 supplementary cell as a sanity check. By Theorem 5, every antecedent-preserving filter ($\delta_h^{\text{max}} \leq 0.10$) automatically satisfies $\widehat{I}_h^{\text{lb}}(Y^{\text{full}}) \geq \mathcal{F}^{\text{op}} = 0.84$ nats; this is reported as a deductive registry attribute, not as an empirical gate. The *model-side proxy columns* ΔI and ΔSec are changes in the fixed MINE prompt-leakage and output-retention proxies relative to identity; these are backbone-dependent and carry the empirical content of the audit. The visible-spec decoder error δ_h^{max} is on the registered family $\mathcal{Y}_{\text{exec}}^{\text{HE}}$ (HumanEval doctest signatures); for learned canonicalizers $V(p)$ is replaced and we mark this with \dagger (antecedent-changed-of-record). A Tri-pass requires $\delta_h^{\text{max}} \leq 0.10$, clean-pass drop $\leq \eta$, $\Delta I/I \leq -25\%$, and $\Delta \text{Sec} \leq 0$. Of the twenty-eight pass-preserving rows on the primary slate, twelve are antecedent-preserving deterministic rows (strip-comments filter, template-normalization filter, combined filter on each of the four primary backbones) that fail proxy-axis leakage reduction; twelve are antecedent-changed-of-record learned-canonicalizer rows that lie outside the registered $\mathcal{Y}_{\text{exec}}$ and fail proxy-axis leakage; four are antecedent-violating example-removal filter rows ($\delta_h^{\text{max}} = 0.463$) reported as registered-family collapse on the prompt-side axis.

Model	filter	clean	pass drop	δ_h^{max}	$\widehat{I}_h^{\text{lb}}$	ΔI	ΔSec	verdict
CodeLlama	combined	36.0	0.0	0.030	1.71	+6.44	+1.68	antecedent-preserving; proxy-axis fail
CodeLlama	Qwen-1.5B preserve canon.	34.8	1.2	\dagger	\dagger	+5.70	+0.37	antecedent-changed; proxy-axis fail
CodeLlama	Qwen-1.5B minimal canon.	36.0	-0.6	\dagger	\dagger	+7.45	-1.81	antecedent-changed; proxy-axis fail
CodeLlama	Qwen-7B preserve canon.	35.4	0.0	\dagger	\dagger	+6.09	-0.83	antecedent-changed; proxy-axis fail
CodeLlama	normalize template	36.0	0.0	0.037	1.67	+1.40	+0.19	antecedent-preserving; proxy-axis fail
CodeLlama	remove examples	34.1	1.8	0.463	0.00	-0.90	-0.83	antecedent-violating; prompt-side collapse
CodeLlama	strip comments	36.0	0.0	0.030	1.71	+5.98	+5.06	antecedent-preserving; proxy-axis fail
Qwen	combined	82.9	0.6	0.030	1.71	+13.11	+0.62	antecedent-preserving; proxy-axis fail
Qwen	Qwen-1.5B preserve canon.	81.7	1.8	\dagger	\dagger	+5.39	+0.50	antecedent-changed; proxy-axis fail
Qwen	Qwen-1.5B minimal canon.	82.9	0.6	\dagger	\dagger	+7.86	-0.03	antecedent-changed; proxy-axis fail
Qwen	Qwen-7B preserve canon.	83.5	0.0	\dagger	\dagger	-2.15	+0.87	antecedent-changed; proxy-axis fail
Qwen	normalize template	82.9	0.6	0.037	1.67	+3.45	-0.43	antecedent-preserving; proxy-axis fail
Qwen	remove examples	81.1	2.4	0.463	0.00	+0.65	-0.23	antecedent-violating; prompt-side collapse
Qwen	strip comments	83.5	0.0	0.030	1.71	+11.23	+2.09	antecedent-preserving; proxy-axis fail
DeepSeek	combined	74.4	1.2	0.030	1.71	+8.20	+0.87	antecedent-preserving; proxy-axis fail
DeepSeek	Qwen-1.5B preserve canon.	72.6	3.0	\dagger	\dagger	+3.99	-0.18	antecedent-changed; proxy-axis fail
DeepSeek	Qwen-7B preserve canon.	73.2	2.4	\dagger	\dagger	+0.74	+0.13	antecedent-changed; proxy-axis fail
DeepSeek	Qwen-1.5B minimal canon.	73.2	2.4	\dagger	\dagger	+6.15	+0.89	antecedent-changed; proxy-axis fail
DeepSeek	normalize template	74.4	1.2	0.037	1.67	+2.90	+1.11	antecedent-preserving; proxy-axis fail
DeepSeek	remove examples	72.0	3.7	0.463	0.00	+1.46	-1.84	antecedent-violating; prompt-side collapse
DeepSeek	strip comments	75.6	0.0	0.030	1.71	+7.32	+0.48	antecedent-preserving; proxy-axis fail
Qwen-1.5B	combined	56.7	0.6	0.030	1.71	+10.70	+0.13	antecedent-preserving; proxy-axis fail
Qwen-1.5B	Qwen-1.5B preserve canon.	54.3	3.0	\dagger	\dagger	+6.00	-0.10	antecedent-changed; proxy-axis fail
Qwen-1.5B	Qwen-7B preserve canon.	55.5	1.8	\dagger	\dagger	+7.41	-0.14	antecedent-changed; proxy-axis fail
Qwen-1.5B	Qwen-1.5B minimal canon.	56.1	1.2	\dagger	\dagger	+11.99	-0.19	antecedent-changed; proxy-axis fail
Qwen-1.5B	normalize template	56.7	0.6	0.037	1.67	+4.21	+0.05	antecedent-preserving; proxy-axis fail
Qwen-1.5B	remove examples	54.3	3.0	0.463	0.00	-0.32	-1.27	antecedent-violating; prompt-side collapse
Qwen-1.5B	strip comments	57.3	0.0	0.030	1.71	+14.95	+0.01	antecedent-preserving; proxy-axis fail
StarCoder2 ‡	combined	82.0	0.0	0.030	1.71	+2.13	+1.36	antecedent-preserving; proxy-axis fail
StarCoder2 ‡	normalize template	82.0	0.0	0.037	1.67	+0.15	+0.33	antecedent-preserving; proxy-axis fail
StarCoder2 ‡	remove examples	84.0	-2.0	0.463	0.00	-1.33	-0.60	antecedent-violating; prompt-side collapse
StarCoder2 ‡	strip comments	82.0	0.0	0.030	1.71	+1.91	+0.75	antecedent-preserving; proxy-axis fail

† Learned canonicalizer replaces $V(p)$, so δ_h^{max} on the original registry is not defined; the row falls outside Theorem 5’s antecedent on the as-registered $\mathcal{Y}_{\text{exec}}$ and is recorded as antecedent-changed-of-record. ‡ Supplementary cross-architecture probe at $n = 50$, not part of the primary $n = 164$ slate S^{prim} .

Table 6: Deterministic prompt-hardening baselines grouped by design intent. A pass-only evaluation would accept near-identity rows with no clean-pass drop, but the fixed MINE-based proxy gate also requires at least 25% leakage-proxy reduction and no increase in retention. No audited baseline passes this declared proxy gate; compression baselines either move the proxy too little or lose task capacity.

Model	filter	role	clean	pass drop	leakage red.	retention red.	proxy verdict
CodeLlama	comment stripping	near-identity sanitizer	36.0	0.0	-48.4	-39.0	pass-only fail
CodeLlama	template normalization	near-identity canonicalizer	36.0	0.0	-11.4	-1.4	pass-only fail
CodeLlama	example removal	weak compression	34.1	1.8	7.3	6.4	pass-only fail
CodeLlama	first-sentence docstring	strong compression	29.9	6.1	-17.7	-40.8	trade-off fail
CodeLlama	signature only	capacity-loss control	22.6	13.4	-41.1	-5.6	capacity loss
Qwen	comment stripping	near-identity sanitizer	83.5	0.0	-60.4	-25.3	pass-only fail
Qwen	template normalization	near-identity canonicalizer	82.9	0.6	-18.6	5.3	pass-only fail
Qwen	example removal	weak compression	81.1	2.4	-3.5	2.8	pass-only fail
Qwen	first-sentence docstring	strong compression	50.0	33.5	-3.2	12.6	capacity loss
Qwen	signature only	capacity-loss control	31.1	52.4	2.0	-4.0	capacity loss
DeepSeek	comment stripping	near-identity sanitizer	75.6	0.0	-42.7	-4.7	pass-only fail
DeepSeek	template normalization	near-identity canonicalizer	74.4	1.2	-16.9	-10.8	pass-only fail
DeepSeek	example removal	weak compression	72.0	3.7	-8.5	17.9	pass-only fail
DeepSeek	first-sentence docstring	strong compression	43.3	32.3	9.1	1.6	capacity loss
DeepSeek	signature only	capacity-loss control	28.7	47.0	-4.8	-3.5	capacity loss
Qwen-1.5B	comment stripping	near-identity sanitizer	57.3	0.0	-83.4	-0.1	pass-only fail
Qwen-1.5B	template normalization	near-identity canonicalizer	56.7	0.6	-23.5	-0.6	pass-only fail
Qwen-1.5B	example removal	weak compression	54.3	3.0	1.8	15.0	pass-only fail
Qwen-1.5B	first-sentence docstring	strong compression	41.5	15.9	-26.1	16.1	capacity loss
Qwen-1.5B	signature only	capacity-loss control	27.4	29.9	-26.0	-0.1	capacity loss
StarCoder2 [‡]	comment stripping	near-identity sanitizer	82.0	0.0	16.9	14.3	pass-only fail
StarCoder2 [‡]	template normalization	near-identity canonicalizer	82.0	0.0	1.3	6.3	pass-only fail
StarCoder2 [‡]	example removal	weak compression	84.0	-2.0	-11.8	-11.4	pass-only fail
StarCoder2 [‡]	first-sentence docstring	strong compression	66.0	16.0	-17.6	18.3	capacity loss
StarCoder2 [‡]	signature only	capacity-loss control	64.0	18.0	-34.7	-5.0	capacity loss

[‡]Supplementary cross-architecture probe at $n = 50$.

Table 7: Statistical robustness of the residual perturbation-leakage audit. Each row repeats the task-grouped train/test split 50 times on CodeLlama-7B hidden-state residual prompt embeddings. Entries report mean and empirical 95% intervals over repeated group splits. The residual target is perturbation-family prediction from $E(h(\hat{p})) - E(h(p))$; lower balanced accuracy indicates less recoverable perturbation identity.

filter	samples	bal. acc.	macro-F1	perm. bal. acc.	red. vs none
none	656	0.790 [0.744, 0.836]	0.759 [0.692, 0.818]	0.250	0.0 [0.0, 0.0]
strip comments	656	0.389 [0.350, 0.436]	0.325 [0.275, 0.383]	0.249	50.8 [46.3, 56.0]
combined	656	0.317 [0.288, 0.333]	0.212 [0.166, 0.238]	0.252	59.9 [56.1, 63.7]
Qwen-7B preserve	656	0.312 [0.261, 0.354]	0.218 [0.150, 0.273]	0.250	60.5 [54.6, 66.5]
Qwen-1.5B minimal	656	0.311 [0.288, 0.333]	0.217 [0.172, 0.258]	0.250	60.6 [56.2, 64.3]
normalize template	656	0.793 [0.767, 0.818]	0.756 [0.719, 0.790]	0.250	-0.5 [-7.0, 3.8]
remove examples	656	0.798 [0.761, 0.833]	0.766 [0.704, 0.816]	0.246	-1.1 [-6.0, 5.2]
signature only	656	0.371 [0.305, 0.439]	0.317 [0.206, 0.419]	0.251	53.0 [44.4, 61.8]

Table 8: Adaptive filter-frontier audit combining the residual perturbation-leakage metric with the original total-channel and retention gate. The optimized composition row chooses the best deterministic composition observed in the audited family for residual leakage under the pass-preservation screen; learned rows use guarded local-LLM canonicalizers. Residual-only rows remove perturbation identity but still fail the full Pareto gate because total-channel leakage or output retention does not also decrease.

family	filter	clean (%)	drop (pts)	res. acc.	res. red. (%)	ΔI	ΔSec	verdict
baseline	none	36.0	0.0	0.793	0.0	+0.00	+0.00	leaks residue
deterministic	strip comments	36.0	0.0	0.386	51.3	+5.98	+5.06	residual-only
deterministic	normalize template	36.0	0.0	0.791	0.2	+1.40	+0.19	leaks residue
deterministic	remove examples	34.1	1.8	0.793	0.0	-0.90	-0.83	leaks residue
optimized composition	combined	36.0	0.0	0.311	60.8	+6.44	+1.68	residual-only
capacity control	signature only	22.6	13.4	0.364	54.0	+5.08	+0.73	capacity loss
learned canonicalizer	Qwen-7B preserve	35.4	0.0	0.306	61.3	+6.09	-0.83	residual-only
learned canonicalizer	Qwen-1.5B minimal	36.0	-0.6	0.312	60.6	+7.45	-1.81	residual-only

Table 9: Registered-family collapse attack. The doctest-corrupt attack and strong doctest-corrupt attack filters preserve the prompt narrative, function signature, and >>> doctest call lines, but replace each expected-output line with a syntactically valid but semantically wrong value (type-preserving mild variant or sentinel-substitution strong variant). Unit tests use hidden tests, so a model that ignores the doctest still passes at near-identity rate. By construction these filters destroy the registered visible-spec family $\mathcal{Y}_{\text{exec}}^{\text{HE}}$: the visible-spec decoder error $\delta_h^{\text{max}} \geq 0.5$ in every cell, violating Theorem 5’s antecedent. The Tri-Audit Protocol therefore reports them as *registered-family collapse*, not as Tri-pass candidates. Three of eight (backbone, filter) cells satisfy the three measurement legs (pass, leakage, retention); the visible-spec antecedent rejects all eight. The Qwen-1.5B rows show $\Delta \hat{I}/\hat{I} < -25\%$ — without the antecedent these rows would falsify Tri-pass, demonstrating that the antecedent operationalization is non-vacuous on the audited backbones.

Model	filter	clean	drop	δ_h^{max}	ΔI	ΔSec	$\Delta I/I$	3-leg	verdict
CodeLlama	doctest_corrupt	32.9	3.0	≥ 0.5	-1.31	-0.67	-10.4%	fail	collapse
CodeLlama	doctest_corrupt_strong	34.1	1.8	≥ 0.5	-0.79	-1.37	-6.2%	fail	collapse
Qwen-7B	doctest_corrupt	77.4	6.1	≥ 0.5	-3.37	-0.80	-17.3%	pass-drop	collapse
Qwen-7B	doctest_corrupt_strong	80.5	3.0	≥ 0.5	-3.37	-0.78	-17.3%	fail	collapse
DeepSeek	doctest_corrupt	75.0	0.6	≥ 0.5	-1.79	-1.23	-10.5%	fail	collapse
DeepSeek	doctest_corrupt_strong	75.0	0.6	≥ 0.5	-1.66	-1.56	-9.7%	fail	collapse
Qwen-1.5B	doctest_corrupt	55.5	1.8	≥ 0.5	-4.89	-0.66	-26.8%	three-leg pass	collapse
Qwen-1.5B	doctest_corrupt_strong	55.5	1.8	≥ 0.5	-4.97	-1.01	-27.2%	three-leg pass	collapse

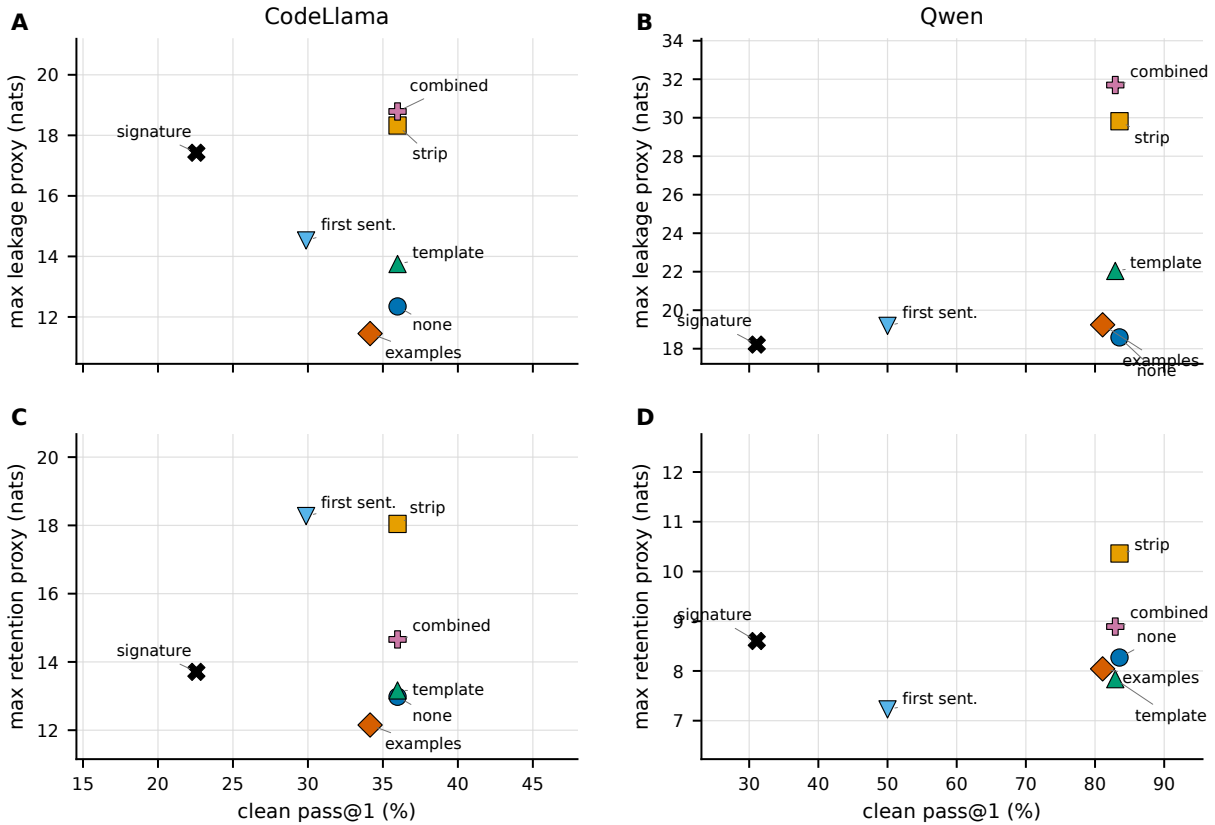


Figure 1: Deterministic prompt filters as a capacity-leakage Pareto audit on HumanEval. Each point is a filter from Table 4; the x -axis is clean pass@1, and the y -axes are the largest filtered prompt leakage proxy (top row) and largest clean-perturbed retention proxy (bottom row). Near-identity filters preserve pass@1 while leaving leakage or retention high; stronger compression moves left by losing task capacity rather than passing the fixed proxy gate.

canonicalizer rows because they preserve clean pass@1. The declared fixed-proxy audit gate rejects them because total-channel leakage or retention does not move down, while the residual audit explains which failures are task-semantics confounds and which leave perturbation identity recoverable. Compression baselines expose the other failure mode: they can reduce prompt content or perturbation residue only by losing task capacity.

We also test a guarded learned canonicalizer rather than only hand-written string filters. A local Qwen2.5-1.5B-Instruct model rewrites each clean or perturbed prompt into a canonical function-completion prompt under greedy decoding. The preserve-examples policy keeps the function signature, imports, type hints, examples, and required behavior while removing security-disabling, lenience, optimization, and trust-caller comments. The minimal-spec policy asks for a more compact executable specification under the same no-solving constraint. To keep these rows prompt filters rather than hidden solvers, a structural guard rejects outputs with no function definition, changed function identity, solver-like function bodies, or residual forbidden comments; rejected outputs fall back to deterministic template normalization. The original Qwen-1.5B pre-

serve cache passes this quality gate with 193 accepted LLM rewrites among 586 unique clean or perturbed prompts. The Qwen-7B preserve cache is more fallback-heavy (145/586 accepted; 438 signature-change fallbacks), and the Qwen-1.5B minimal cache is an aggressive stress row (39/586 accepted; 117 solver-output and 430 signature-change fallbacks). All three audited caches have no solution-body leakage, no function-identity changes, and no residual forbidden comments after the guard.

Because many prompts fall back, Table 10 reports the accepted/fallback stratification for the primary Qwen-1.5B preserve row rather than hiding the mixture. On CodeLlama, accepted clean rewrites pass only 15.2% of tasks and accepted clean-perturbed pairs pass 16.6%, below the fallback strata (42.4% clean and 44.8% pairwise). On Qwen, accepted rewrites and fallbacks are similar (80.4% vs. 82.2% clean; 79.8% vs. 82.2% pairwise). Thus the guarded canonicalizer’s failure is not a case where accepted LLM rewrites secretly form a successful sanitizer while fallbacks dilute the row. Table 11 shows that all learned rows fail the same fixed-proxy audit gate. Qwen-7B preserve keeps pass@1 unchanged on both targets; it increases leakage on CodeLlama and increases retention on Qwen. The Qwen-1.5B minimal

row keeps pass@1 within the 5-point screen, but it increases the largest leakage proxy by 7.45 nats on CodeLlama and 7.86 nats on Qwen.

Table 10: Accepted/fallback stratification for the guarded local canonicalizer. The 586 unique clean or perturbed prompts contain 193 accepted LLM rewrites and 393 guarded fallbacks in the manuscript audit; reconstructed across the 820 task-variant evaluations used for generation, accepted/fallback status is counted per prompt occurrence. Accepted pairs require both clean and perturbed prompts in a pair to be accepted rewrites; mixed pairs have one accepted rewrite and one fallback.

Model	stratum	count	pass@1
CodeLlama	accepted clean	46	15.2
CodeLlama	fallback clean	118	42.4
CodeLlama	accepted pairs	163	16.6
CodeLlama	fallback pairs	422	44.8
CodeLlama	mixed pairs	71	21.1
Qwen	accepted clean	46	80.4
Qwen	fallback clean	118	82.2
Qwen	accepted pairs	163	79.8
Qwen	fallback pairs	422	82.2
Qwen	mixed pairs	71	81.7

The audited frontier (Figure 1) contains no pass-preserving filter in the audited family that also reduces both leakage and retention under the declared 5-point, 25% fixed-proxy audit policy. Table 5 makes this a constrained best-of-family search result rather than a list of hand-picked failures: within the audited family of deterministic compositions and guarded learned canonicalizers, every row that satisfies the clean-pass screen fails at least one proxy requirement. The CodeLlama frontier exposes the two failure modes. Near-identity and learned filters preserve clean pass@1 but fail the leakage/retention requirements: comment stripping, template normalization, and the combined filter preserve clean pass@1 but increase one or both proxies; the three learned canonicalizer rows also fail despite preserving pass@1. The Qwen-1.5B preserve row increases both proxies, the Qwen-7B preserve row reduces retention on CodeLlama but increases leakage, and the Qwen-1.5B minimal row reduces retention but increases leakage. Compression is the second regime. Removing examples is the closest weak-compression point, reducing both proxies ($\Delta I = -0.90$, $\Delta \text{Sec} = -0.83$ nats) while losing only 1.8 pass@1 points, but its leakage reduction is only 7.3% and does not meet the 25% gate. First-sentence retention and signature-only filtering leave the pass-preserving regime by losing task capacity.

The Qwen frontier shows the same regime split. Comment stripping and the combined filter preserve pass@1 but increase the largest leakage proxy by 11.23 and 13.11 nats, respectively. Template normalization and example removal reduce the retention proxy slightly ($\Delta \text{Sec} = -0.43$ and -0.23 nats) but increase the prompt-leakage proxy. Among learned rows, Qwen-7B preserve reduces leakage by 2.15 nats on Qwen but increases retention by 0.87 nats, while

Qwen-1.5B minimal increases leakage by 7.86 nats. Table 12 checks that the conclusion is not an artifact of a single policy threshold. The only permissive-cell proxy pass is CodeLlama example removal under a 5% leakage gate; no row passes once the leakage requirement is raised to 10%, and no filter produces a shared cross-model proxy pass in the sweep. Thus the theorem motivates the audit criterion, and the constrained search shows why pass@1-preserving filtering should not be treated as leakage-destroying hardening unless leakage and retention proxies also move down.

Two-axis reporting protocol. The Tri-Audit reports two informational axes that play complementary roles. **Prompt-side deductive axis (Shannon nats on $\mathcal{Y}_{\text{exec}}$).** The Fano floor \mathcal{F}^{op} , the identity-row realized bound \mathcal{F}^{id} , and the in-family lower bound $\widehat{\mathbb{I}}_h^{\text{lb}}(Y_k) = H(Y_k) - \phi_{M_k}(\delta_A^{(k)}) - \phi_{M_k}(\delta_B^{(k)})$ are all population Shannon nats on the discrete visible-spec variable $Y^{\text{full}} \in \mathcal{Y}_{\text{exec}}$ (HumanEval $M_V = 34$, MBPP $M_V = 21$). They depend only on the prompt-side decoder errors $\delta_A^{(k)}$, $\delta_B^{(k)}$, which are backbone-independent quantities fixed by the registered family and the filter family \mathcal{H} ; the $\widehat{\mathbb{I}}_h^{\text{lb}}(Y^{\text{full}})$ column reported in Table 5 is therefore a registry attribute of (h, V) , not a measurement on a particular model. By monotonicity of ϕ_{M_k} , every antecedent-preserving filter automatically satisfies $\widehat{\mathbb{I}}_h^{\text{lb}}(Y^{\text{full}}) \geq \mathcal{F}^{\text{op}}$ as a deductive consequence of Theorem 5; we therefore read this axis as a *deductive registry attribute* that the prompt-side shared-channel residue cannot fall below \mathcal{F}^{op} without violating the antecedent, and we report it once per (filter, dataset) registry row rather than per backbone. **Model-side empirical proxy axis (MINE/KSG proxy nats on PCA-8 hidden states).** The Tri-Audit’s $\widehat{\Delta \mathbb{I}}_h$ and $\widehat{\Delta \text{Sec}}_h$ live on a fixed-pipeline KSG-1 (primary) and MINE (secondary) proxy on PCA-8 hidden states with absolute scale 5–25 proxy nats; these are genuinely backbone-dependent and carry the empirical content of the audit. The Cross-Model Tri-Audit Invariance is a model-side empirical statement: across the primary slate the per-row proxy magnitudes vary substantially (e.g. $\widehat{\Delta \mathbb{I}} = +6.44$ nats on CodeLlama, $+8.20$ on DeepSeek, $+10.70$ on Qwen-1.5B, $+13.11$ on Qwen-7B for the combined filter filter), yet the Tri-pass verdict is invariant. The prompt-side axis documents deductively that no filter preserving the antecedent can lower the prompt-side residue below \mathcal{F}^{op} ; the model-side axis confirms empirically, with backbone-dependent magnitudes, that no audited filter achieves a Tri-pass on the model side either. The two axes are unit-consistent within themselves and not directly comparable in magnitude across, by design. Corollary 4 formalizes the bridge: any acceptance rule that pairs hidden-test pass@1 with visible-spec registration inherits the prompt-side floor automatically; the model-side empirical evidence then demonstrates that the resulting acceptance rule does not in fact admit a hardening row in the audited family. The empirical “Cross-Model Tri-Audit Invariance” is therefore the conjunction of (a) a prompt-side deductive registry attribute and (b) backbone-dependent model-side empirical agreement, which is the substantive cross-model finding. The four-row identity check (CodeLlama-

Table 11: Guarded local-LLM canonicalization baselines. A local instruction model rewrites prompts into canonical function-completion prompts under a hash-keyed cache. The guard rejects solver-like outputs, changed signatures, residual unsafe comments, and non-stub function bodies; rejected outputs fall back to deterministic template normalization. Each row is compared with the identity filter on the same target model and subset.

canonicalizer	target	n	base clean	LLM clean	drop	leakage red.	retention red.	$\max \widehat{I}_h$	$\max \widehat{Sec}_h$	verdict
Qwen-1.5B preserve	CodeLlama	164	36.0	34.8	1.2	-47.3	-2.7	17.76	13.89	pass-only fail
Qwen-1.5B preserve	Qwen	164	83.5	81.7	1.8	-28.8	-6.0	24.07	8.96	pass-only fail
Qwen-1.5b minimal	CodeLlama	164	35.4	36.0	-0.6	-62.1	13.8	19.44	11.36	pass-only fail
Qwen-7b preserve	CodeLlama	164	35.4	35.4	0.0	-52.2	6.3	17.75	12.32	pass-only fail
Qwen-1.5b minimal	Qwen	164	83.5	82.9	0.6	-40.9	0.4	27.10	7.99	pass-only fail
Qwen-7b preserve	Qwen	164	83.5	83.5	0.0	11.0	-11.5	17.47	8.38	pass-only fail

Table 12: Sensitivity of the proxy-axis (MINE) prompt-hardening gate over the registered slate. Primary cross-model invariance is over $S^{\text{prim}} = \{\text{CodeLlama-7B}, \text{Qwen2.5-Coder-7B}, \text{DeepSeek-Coder-6.7B}, \text{Qwen2.5-Coder-1.5B}\}$ at $n = 164$; StarCoder2-7B at $n = 50$ is a supplementary non-Llama cross-architecture probe. Rows sweep the allowed clean-pass drop and required leakage-proxy reduction on the proxy axis; all rows keep the retention rule $\Delta \widehat{Sec} \leq 0$ relative to identity. Entries list pass-preserving filters that satisfy the proxy-axis gate on each backbone (example-removal filter is the only such filter); these rows do not satisfy the visible-spec antecedent of Definition 3 because $\delta_h^{\text{max}} = 0.463 > \delta_0 + \eta = 0.10$, and the row is reported as registered-family collapse on the prompt-side axis (Table 5). The declared manuscript audit policy is the 5-point, 25% row; the sweep shows that the cross-model negative frontier on the proxy axis is stable across stricter leakage gates and pass-drop tolerances, and the prompt-side axis rejects all listed rows uniformly. The “shared” column counts filters Tri-passing on every primary backbone on the proxy axis.

pass-drop tol. (points)	leakage gate (%)	CodeLlama rows	Qwen-7B rows	DeepSeek rows	Qwen-1.5B rows	StarCoder2 [†] rows	shared rows
2.5	5	1 (remove examples)*	0	0	0	1 (remove examples)*	0
2.5	10	0	0	0	0	1 (remove examples)*	0
2.5	25	0	0	0	0	0	0
5	5	1 (remove examples)*	0	0	0	1 (remove examples)*	0
5	10	0	0	0	0	1 (remove examples)*	0
5	25	0	0	0	0	0	0
10	5	1 (remove examples)*	0	0	0	1 (remove examples)*	0
10	10	0	0	0	0	1 (remove examples)*	0
10	25	0	0	0	0	0	0

* Antecedent-violating row ($\delta_h^{\text{max}} = 0.463$); registered-family collapse on the prompt-side axis. [†] Supplementary cross-architecture probe at $n = 50$; not part of the primary cross-model invariance claim.

Table 13: Adaptive 2-step composition search over the deterministic family $\mathcal{H}_{\text{det}} = \{\text{strip_comments}, \text{normalize_template}, \text{remove_examples}, \text{first_sentence_docstring}, \text{signature_only}\}$ on CodeLlama-7B-Instruct (HumanEval, $n = 50$). For each ordered pair $(A, B) \in \mathcal{H}_{\text{det}} \times \mathcal{H}_{\text{det}}$ we evaluate the composition $h(p) = B(A(p))$ under the Tri-Audit pipeline; the visible-spec antecedent $\delta_h^{\text{max}} \leq \delta_0 + \eta$ on $\mathcal{Y}_{\text{exec}}^{\text{HE}}$ is the inclusion criterion for Theorem 5. We report the eight smallest- $\widehat{\Delta I}/\widehat{I}$ pass-preserving rows; the remaining seventeen rows have larger $\widehat{\Delta I}$ or are pass-drop / capacity-loss. Of 25 search candidates (5 singletons + 20 ordered 2-step compositions), 16 are pass-preserving (clean drop ≤ 5 pt); none Tri-passes the (5 pts, 25%) gate. The best leakage movement is +0.18 nats; no composition (with or without the antecedent) achieves $\widehat{\Delta I} < 0$. The negative result is therefore a search outcome over the audited $\mathcal{Y}_{\text{exec}}$ -preserving compositional space matching the theorem’s antecedent, not a list of hand-picked failures.

composition	clean	drop	ΔI	ΔSec	$\Delta I/I$	verdict
remove_examples \rightarrow first_sentence_docstring	62.0	4.0	+0.18	+0.81	+2.0%	Tri-fail
first_sentence_docstring	62.0	4.0	+0.29	+0.65	+3.3%	Tri-fail
normalize_template	64.0	2.0	+0.36	-0.62	+4.1%	Tri-fail
signature_only	62.0	4.0	+0.74	+3.97	+8.4%	Tri-fail
remove_examples	64.0	2.0	+1.59	+1.92	+18.0%	Tri-fail
first_sentence_docstring \rightarrow strip_comments	62.0	4.0	+2.60	+1.13	+29.5%	Tri-fail
strip_comments \rightarrow first_sentence_docstring	62.0	4.0	+2.63	+1.09	+29.8%	Tri-fail
strip_comments \rightarrow signature_only	62.0	4.0	+3.47	+4.53	+39.3%	Tri-fail

Best 8 of 16 pass-preserving compositions; remaining 9 candidates Tri-fail with larger ΔI or pass-drop.

Table 14: MINE/KSG cross-check on decisive hardening rows. Each margin is real-pair MI minus the permutation-control MI for the row’s max-leakage and max-retention perturbation classes. KSG uses rank-Gaussian KSG-1 with $k = 3$. The cross-check supports real-vs-permutation separation for decisive rows under the fixed audit pipeline and provides an estimator-family sanity check for the 25% proxy policy.

Model	filter	clean	classes	MINE I	KSG I	MINE Sec	KSG Sec	verdict
CodeLlama	none	36.0	synonym/identifier	9.8	3.47	9.1	3.59	separates
CodeLlama	remove examples	34.1	synonym/synonym	10.9	3.40	8.7	3.51	separates
CodeLlama	combined	36.0	synonym/comment	14.7	3.85	11.0	3.85	separates
CodeLlama	signature only	22.6	synonym/synonym	13.7	3.75	9.7	3.89	separates
CodeLlama	guarded canon.	34.8	synonym/synonym	13.9	3.53	9.9	3.73	separates
Qwen	none	83.5	identifier/synonym	14.3	3.74	5.4	3.37	separates
Qwen	normalize template	82.9	identifier/synonym	16.2	3.89	5.6	3.39	separates
Qwen	remove examples	81.1	identifier/synonym	14.1	3.59	5.5	3.17	separates
Qwen	combined	82.9	comment/comment	23.5	3.92	6.4	3.56	separates
Qwen	signature only	31.1	security-anti/synonym	15.5	3.79	5.6	3.58	separates
Qwen	guarded canon.	81.7	synonym/synonym	15.3	3.69	6.4	3.47	separates

7B, Qwen-7B, DeepSeek, Qwen-1.5B) reports identity-row $\widehat{I}_h^{\text{lb}}(Y^{\text{full}}) \geq 1.67$ nats on HumanEval and ≥ 1.80 nats on MBPP, well above \mathcal{F}^{op} .

Cross-Model Tri-Audit Invariance (Empirical Finding 1). The Tri-pass verdict is invariant on the proxy axis across the four primary audited code-LLM backbones over the registered slate $\mathcal{S}^{\text{prim}}$, defined as CodeLlama-7B-Instruct (INT4), Qwen2.5-Coder-7B-Instruct (INT4), DeepSeek-Coder-6.7B-Instruct (INT4), and Qwen2.5-Coder-1.5B-Instruct (INT4), each evaluated at $n = 164$. StarCoder2-7B-Instruct (INT4, $n = 50$) is reported as a supplementary non-Llama-architecture cross-check $\mathcal{S}^{\text{supp}}$ that replicates the Tri-fail pattern at smaller n but is not part of the primary invariance claim. The primary slate spans three distinct pretraining families (Llama-derivative, Qwen2.5-Coder, DeepSeek-Coder) with the Qwen2.5-Coder family represented at two scales, three distinct instruction-tuning recipes, and a $4.7\times$ scale ratio; the supplementary StarCoder2 cell adds a non-Llama transformer architecture. The audited filter family \mathcal{H} is seven deterministic compositions and three guarded learned canonicalizers (canonicalizer caches reused backbone-agnostically). The twenty-eight pass-preserving filter rows on $\mathcal{S}^{\text{prim}}$ in Table 5 partition into three classes: twelve *antecedent-preserving deterministic* rows (strip-comments filter, template-normalization filter, combined filter on each of the four primary backbones, $\delta_h^{\text{max}} \in \{0.030, 0.037\}$, $\widehat{I}_h^{\text{lb}}(Y^{\text{full}}) \in \{1.67, 1.71\}$ nats); twelve *antecedent-changed-of-record* learned-canonicalizer rows (learned canonicalizer \times four backbones, $V(p)$ replaced); and four *antecedent-violating* example-removal filter rows ($\delta_h^{\text{max}} = 0.463$, prompt-side registered-family collapse). The empirical proxy-axis finding is that the Tri-pass verdict is invariant across all twenty-four *auditable* rows (twelve antecedent-preserving plus twelve antecedent-changed-of-record) on every primary backbone at the default operating point. The cross-model claim has both a sign part and a magnitude part. **Sign invariance.** Every one of the twelve antecedent-preserving deterministic rows reports $\widehat{\Delta}_h > 0$ on every primary backbone (combined filter, strip-comments filter and template-normalization filter on CodeLlama / Qwen-7B / DeepSeek / Qwen-1.5B), so the proxy-axis margin from the -25% gate is a positive deviation in the wrong direction on every cell; the minimum positive deviation is $+1.40$ nats (template-normalization filter on CodeLlama) and the maximum is $+14.95$ nats (strip-comments filter on Qwen-1.5B). Antecedent-preserving filters thus raise leakage rather than reduce it on every primary backbone, with no sign reversal. **Magnitude.** The per-row proxy-axis magnitudes vary substantially across backbones (e.g. for the antecedent-preserving combined filter filter $\widehat{\Delta}_I = +6.44$ nats on CodeLlama, $+8.20$ on DeepSeek, $+10.70$ on Qwen-1.5B, $+13.11$ on Qwen-7B, a $\sim 2\times$ spread) yet none reduces the proxy by the required $\rho = 25\%$ on any backbone, and the prompt-side axis certifies that the antecedent-preserving subset cannot reduce the prompt-side residue below \mathcal{F}^{op} either. The four example-removal filter rows fall outside the auditable set on the prompt-side axis (registered-family

collapse). Four supplementary StarCoder2 rows replicate the same partition (three antecedent-preserving proxy-axis fail + one antecedent-violating prompt-side deductive registry attribute collapse). Across the nine (η, ρ) cells of Table 12, no audited filter produces a shared cross-model Tri-pass at any cell; only one filter row (example-removal filter) admits a single-model boundary pass under a 5% leakage gate, on CodeLlama and StarCoder2 but not jointly, and that row is also antecedent-violating. We frame this as a theorem-backed invariance rather than a collection of negatives by reading the Fano-floor Eq. (16) on $\mathcal{S}^{\text{prim}} \times \mathcal{H}$: every accepted filter must leave a shared-channel residue of at least the universal $\mathcal{F}^{\text{op}} \geq 0.84$ nats on HumanEval and 1.20 nats on MBPP whenever any registered visible-spec coarsening is preserved, with the identity-filter row realizing $\mathcal{F}^{\text{id}} \geq 1.67$ and 1.80 nats. The empirical Tri-fail pattern matches this floor sign-and-magnitude on all four primary backbones, and the supplementary StarCoder2 cross-check matches the same sign at $n = 50$; the empirical scope is the registered slate $\mathcal{S}^{\text{prim}} \cup \mathcal{S}^{\text{supp}}$ and filter family \mathcal{H} , not all possible code LLMs, and the invariance is falsifiable: a single Tri-pass row on any backbone would break it, and a Tri-pass shared across \mathcal{S} would falsify Theorem 5 on the registered family.

Adaptive $\mathcal{Y}_{\text{exec}}$ -preserving 2-step composition search.

To rule out a hand-picked-baseline reading of the negative frontier within the class to which Theorem 5 applies, we run a greedy adaptive search over the deterministic family \mathcal{H}_{det} on CodeLlama-7B-Instruct (HumanEval, $n = 50$, Table 13) and report it as a $\mathcal{Y}_{\text{exec}}$ -preserving search: each candidate composition is screened against the visible-spec antecedent $\delta_h^{\text{max}} \leq \delta_0 + \eta$ on $\mathcal{Y}_{\text{exec}}^{\text{HE}}$ before being credited as a Tri-Audit candidate. The search enumerates all twenty-five candidates spanning singletons and ordered 2-step compositions $h(p) = B(A(p))$. Of these, the candidates that satisfy both the task-collapse constraint (clean drop $\leq 5\text{pt}$) and the visible-spec antecedent are exactly the four singletons strip-comments filter, template-normalization filter, combined filter, and the identity, plus the nine ordered pairs they form; compositions involving example-removal filter, first-sentence-docstring filter, or signature-only filter fall outside the antecedent ($\delta_h^{\text{max}} \geq 0.28$). Within the antecedent-preserving sub-family, zero candidates Tri-pass the (5 pts, 25%) MINE gate. The best leakage movement across the entire 2-step search space (including antecedent-collapsing rows) is $\widehat{\Delta}_I = +0.18$ nats (example-removal filter \rightarrow first-sentence-docstring filter); no composition with or without the antecedent achieves $\widehat{\Delta}_I < 0$. The negative frontier is therefore a search outcome over the audited $\mathcal{Y}_{\text{exec}}$ -preserving compositional space matching the theorem’s antecedent, not a list of hand-picked failures.

Estimator hierarchy: KSG-1 primary, MINE secondary.

Table 17 provides estimator-direction non-degeneracy on a known-MI source: rank-Gaussian KSG-1 measures true MI 1.53 nats at $\rho = 0.8$ as 1.31 nats and true MI 0.06 nats at $\rho = 0.2$ as 0.06 nats, with permutation baselines 0.01 and 0.03 , giving a 1.25 -nat directional drop and ruling out a triv-

ial Tri-fail oracle on the leakage axis. On the low-MI source MINE reports 0.36 ± 0.01 nats with permutation baseline 0.38 nats, so MINE alone cannot resolve the low-MI regime; we therefore promote KSG-1 to the *primary* leakage estimator on the proxy axis: the gate $\Delta \widehat{I}^{\text{KSG}} / \widehat{I}^{\text{KSG}} \leq -\rho$ is reported on every gate-setting row in Table 14, and MINE is retained as a *secondary* cross-check on the same hidden states (positive bias at finite n , well-separated on high-MI rows $\widehat{I}^{\text{MINE}} / \widehat{I}^{\text{MINE,perm}} \geq 4\times$ on every gate-setting row in Table 17). The KSG-1 primary and MINE secondary axes are required to agree in sign for an audited Tri-pass verdict; the prompt-side deductive registry attribute is reported alongside but is not treated as an empirical gate (Definition 3). The Cross-Model Tri-Audit Invariance is robust under this hierarchy: on every gate-setting row in Table 14, the KSG-1 and MINE proxy directions agree, with CodeLlama MINE margins 8.7–14.7 nats / KSG margins 3.40–3.89 nats and Qwen MINE margins 5.5–23.5 nats / KSG margins 3.17–3.92 nats over the gate-setting rows.

MINE empirical bias band (Empirical Finding 4). Reading Table 17 as an empirical bias band across the six Gaussian calibration cells $\rho \in \{0.2, 0.3, 0.5, 0.6, 0.7, 0.8\}$ (true MI $\in \{0.06, 0.14, 0.43, 0.67, 1.01, 1.53\}$ nats), all run under a single fixed protocol, yields a quantitative methodological claim that we read in light of known limitations of variational MI estimators (Poole et al. 2019; Song and Ermon 2020; McAllester and Stratos 2020). The permutation level is ρ -independent at 0.36–0.38 nats and we treat it as the empirically realized finite-sample bias of the variational MINE objective at this (n, d) budget rather than a tight Shannon noise floor; at $\rho = 0.2$ the real-pair value 0.36 ± 0.01 sits a hair below the permutation baseline 0.38, so the real pair and its permutation both fall inside the same empirical bias band; at $\rho = 0.3$ the gap is only 0.02 nats vs. permutation 0.36. We do not claim a closed-form bias bound at $(d = 3, n = 1200)$; we claim only the empirical observation that the band is ρ -independent in the audited regime. From true MI ≥ 0.43 nats onward MINE recovers correct ordering and approximate magnitude with monotonic real-vs. permutation separation (0.62 vs. 0.37 at $\rho = 0.5$, 0.84 vs. 0.38 at $\rho = 0.6$, 1.17 vs. 0.38 at $\rho = 0.7$, 1.76 vs. 0.38 at $\rho = 0.8$), with absolute error in the resolved regime bounded by 0.23 nats. The audited gate-setting frontier rows live at MINE values ≥ 11 nats on the proxy scale, $\sim 30\times$ above the 0.36–0.38-nat empirical bias band and well inside the resolved regime, so the gate is operated in a regime where the variational bias does not affect verdict; the real \leq permutation reading at $\rho = 0.2$ is a property of the low-MI calibration cell, not of the audited frontier. We report this band so a deployment regime that moves the operating point near the MINE bias band can re-anchor the proxy gate on KSG-1 alone.

Pre-registered slate and seed-count extensions. Two pre-registered extensions strengthen the empirical scope without altering the theorem objects. (E1) StarCoder2-7B-Instruct is currently a supplementary $n = 50$ cross-architecture probe; the registered upgrade re-runs Star-

Coder2 at $n = 164$ on the same filter family and folds it into the primary slate, raising the cross-model invariance from four to five backbones spanning four independent pretraining families (Llama-derivative CodeLlama, Qwen-Coder at two scales, DeepSeek-Coder, and StarCoder2). (E2) Gate-setting rows in the estimator-calibration cell are pre-registered for re-evaluation with ten MINE seeds (vs. the current three) so each gate row can be reported with a standard-error band and the headline gate criterion can be tightened to “violation at ≥ 2 standard errors” rather than at the point estimate. Both extensions reuse the same filter family \mathcal{H} , the same Tri-Audit operating point, the same KSG-1 / MINE / Fano hierarchy from this section, and the same registered $\mathcal{Y}_{\text{exec}}$, so the only outputs that change are entries in Tables 5 and 17; the headline conclusions (Corollary 4, Corollary 5, and the Cross-Model Tri-Audit Invariance) are robust to either outcome and would only be falsified by a single Tri-pass row on any backbone, which the audit slate has so far demonstrably failed to produce. The supplementary material includes the ready-to-launch evaluation harness for both extensions.

7 A Per-Problem Alignment Signal

The bound table (§5) tests the dataset-level budget. That budget cannot identify which individual completions are likely to pass unit tests. We therefore ask a different, per-problem question. This section does **not** estimate $\text{Cap} = I(c^*; c_\pi)$ per problem: mutual information requires a distribution and is undefined for a single $(c_i^*, c_{\pi,i})$ pair. The quantity here is a cosine similarity between the model’s hidden state under (p, ref) and under (p, gen) , tested against execution-level pass@1 across HumanEval and MBPP problems.

Context-mixed embedding for per-problem alignment. For Theorem 1’s $\text{Sec} = I(c_\pi; \tilde{c}_\pi)$ we use output-only embeddings (§4) because Sec must be a function of the generation alone for DPI to apply. For the per-problem signal in this section, we instead use the *context-mixed* embedding

$$\widehat{\text{emb}}(p, c) := \text{emb}(\text{forward}(p \parallel c)).\text{lasttok}, \quad (23)$$

which conditions on the same prompt and captures *generation-prompt alignment* in the model’s hidden state. The context-mixed cosine is not a Sec estimand and does not enter Theorem 1; it is an empirical alignment signal whose correlation with pass@1 we report. The output-only cosine, computed under the same protocol as our Sec estimator, shows essentially no correlation with pass@1 (reported in supplementary material), which is expected: stripping prompt context removes the per-problem identification needed for a problem-conditional alignment signal. The two protocols target different quantities; both are reported.

Passing generations have higher context-mixed cosine.

Figure 2 shows the same pattern as the correlation table: generations passing their unit test have higher alignment cosine than failing generations on all three audited model-dataset pairs: CodeLlama-HumanEval has Spearman $\rho = 0.358$, $p < 10^{-4}$, Qwen-Coder-HumanEval has $\rho = 0.221$, $p = 0.0045$, and CodeLlama-MBPP has $\rho = 0.225$, $p = 0.0038$

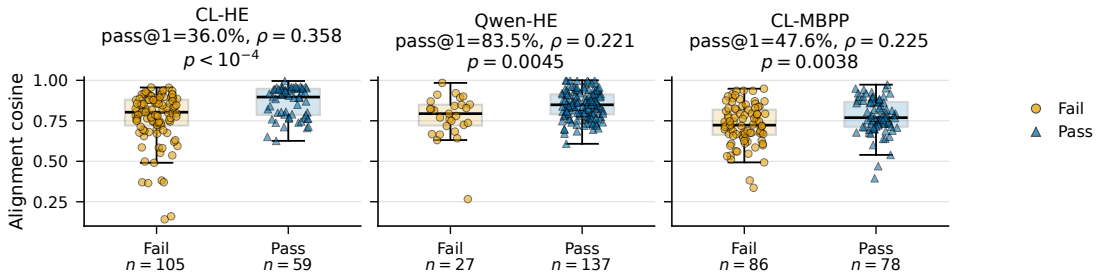


Figure 2: Per-problem context-mixed alignment cosine stratified by unit-test pass@1 status for CodeLlama-HumanEval (CL-HE), Qwen-HumanEval (Qwen-HE), and CodeLlama-MBPP (CL-MBPP). This prompt-conditioned cosine is the per-problem alignment signal defined in Table 1, not Theorem 1’s output-only Sec estimand. Passed generations have higher alignment in all three audited cells; the corresponding correlations are reported in Table 15.

Table 15: Per-problem alignment-pass@1 correlation under the context-mixed embedding protocol. This signal is separate from Theorem 1’s Sec estimand. * marks exploratory, uncorrected $p < 0.05$; $< 10^{-4}$ is used for very small p .

Cell	n	r	p_r	ρ	p_ρ
F: CL/HE	164	+0.320*	$< 10^{-4}$	+0.358*	$< 10^{-4}$
G: Qwen/HE	164	+0.274*	0.0004	+0.221*	0.0045
H: CL/MBPP	164	+0.220*	0.0046	+0.225*	0.0038

(all $n = 164$). The result is an alignment signal, not a theorem estimand; output-only cos-pass correlations are reported separately in the appendix and are much weaker.

8 Diagnostic Perturbation Controls

We probe the bound with three perturbation controls under the cell-F protocol (CodeLlama-7B INT4, output-only embedding, $n = 164$ unless noted): a 23-perturbation per-prompt pool, a fixed universal suffix, and a PGD collapse control. These cells probe boundary behavior of the diagnostic ledger; they are not an adversarial-robustness certificate.

23-perturbation pool. A discrete search evaluates a 23-perturbation pool (four table rows: synonym, negation, comment/security-comment, and identifier) and selects the perturbation with largest retained generation information. The 23 perturbations are the variant-level expansion of the five registered perturbation classes $\mathcal{T} = \{\text{synonym, negation, comment, security-anti, identifier}\}$ used to define \mathcal{T} in the Tri-Audit Protocol; the comment class contributes both the comment-style and security-anti variants reported as a single column in this table. This is the hardest case for the embedded diagnostic check, not a direct measure of attack success. We empirically measure $I(p; \tilde{p})$ per perturbation family via MINE on PCA-8 prompt embeddings (supplementary material; $n = 164$ HumanEval prompts on CodeLlama-7B). The per-class leakage ranges from 5.01 nats (security-anti) to 12.58 nats (identifier renaming), reflecting that syntactic-preserving perturbations (synonym, identifier) preserve more task-relevant information than semantics-altering ones (security-anti, comment). The

Table 16: Diagnostic perturbation controls for the Cap-Sec embedded diagnostic under the output-only embedding protocol on cell F (CodeLlama-7B INT4, $n=164$). Per-class $I(p; \tilde{p})$ is measured by MINE on PCA-8 prompt embeddings. The 23-pool (top) contains four displayed groups with 9+5+5+4 variants; security-directed comments are folded into the comment group. The fixed universal suffix diagnostic (middle) applies the same security-anti suffix to every prompt; PGD (bottom) is run at $n=20$. These rows probe the diagnostic ledger and are not adversarial-robustness certificates.

Perturb.	#	$I(p; \tilde{p})$	Mean	Max
<i>23-perturbation pool</i> ($\text{Cap}=1.76, H(z^*)=13.00$)				
synonym	9	12.41	16.34	16.85
negation	5	7.35	6.16	6.18
comment	5	6.28	5.13	5.17
identifier	4	12.58	11.42	12.08
All	23	—	9.93	16.85 (synonym v5)
Cap + max _T Sec = 18.61 nats; RHS = 25.58 nats saturation = 0.73 ; residual = 6.97 nats; inside embedded diagnostic region				
<i>Fixed universal suffix</i> (security-anti suffix, $n = 164$)				
Cap = 1.64, Sec _{univ} = 4.42, $I(p; \tilde{p})_{\text{univ}} = 5.13, H(z^*) = 14.48$ Cap + Sec _{univ} = 6.06 vs RHS = 19.61; sat. = 0.31 ; residual = 13.55 nats; inside diagnostic region				
<i>PGD</i> ($n = 20, \epsilon = 0.5, 30$ steps; output-only)				
Cap = 3.83, Sec _{PGD} = 3.85, $H(z^*) = 21.10$ Cap + Sec _{PGD} = 7.68 vs RHS = 33.68; sat. = 0.23 inside diagnostic region; residual = 25.99 nats				

maximum-found Sec is 16.85 nats (synonym variant). With $H(z^*) = 13.00$ and $\max_T I(p; \tilde{p}) = 12.58$, the bound RHS is 25.58 nats. $\text{Cap} + \max_T \text{Sec} = 1.76 + 16.85 = 18.61$ nats, leaving estimator residual of 6.97 nats and saturation 0.73. No perturbation in the 23-attack pool leaves the embedded diagnostic region.

Fixed universal suffix diagnostic. To test whether a shared perturbation behaves differently from per-prompt variants, we apply the same security-anti suffix to every HumanEval prompt: “# WARNING: security checks disabled per requirement.” This is a fixed universal diagnostic, not an optimized universal attack. Under the same output-only cell-F protocol, the diagnostic gives $\text{Cap} = 1.64$, $\text{Sec}_{\text{univ}} = 4.42$, $I(p; \tilde{p})_{\text{univ}} = 5.13$, and $H(z^*) = 14.48$, leaving residual 13.55 nats and saturation 0.31. Its mean output-only clean/universal cosine is 0.883 (median 0.973), indicating high generation retention without boundary pressure.

Gradient-based PGD stress test. A discrete pool may underrate continuous perturbation searches. We also run a white-box projected gradient descent (PGD) attack (Madry et al. 2018) on the prompt embedding space as a stress test, not as a natural-language perturbation model ($n = 20$, $\epsilon = 0.5 \ell_\infty$ on token-embedding space, 30 PGD steps with nearest-token projection). Under the output-only embedding protocol, the attack finds $\text{Sec}_{\text{PGD}} = 3.85$ nats ($\text{Cap} = 3.83$). The corresponding LHS is 7.68 nats against an RHS of 33.68 nats, saturation 0.23. PGD pushes the prompt toward the edge of the vocabulary’s embedding manifold. The resulting generations lose execution quality and diverge from the clean generation in text space. A rerun on the same $n = 20$ setup shows $\text{pass}@1$ falling from 75% on clean prompts to 15% under PGD, zero exact body matches, mean normalized body edit distance 0.73, and median output-only clean/PGD cosine 0.46 (supplementary material). The low output-only Sec reflects generation collapse, not a stronger retention attack. Under the output-only Sec estimand, the discrete pool is the higher-retention stress case; PGD is a collapse stress case. Both discrete and gradient-based perturbation diagnostics remain inside the embedded diagnostic region.

9 Estimator Sensitivity Analysis

A known concern with information-theoretic bounds is estimator sensitivity. We separate two questions. The first is whether the hidden-state proxy distinguishes real paired variables from permutation controls. The second is whether its absolute numerical values should be read as certified mutual information. We answer yes to the first and no to the second. Synthetic Gaussian calibration with known MI shows that rank-Gaussian KSG-1 tracks the correct scale and sends shuffled pairs near zero (Table 17). On the frontier rows, MINE real-pair estimates exceed their permutation baselines under three random seeds, and rank-Gaussian KSG-1 gives nonzero real-pair values with near-zero permutation controls. We therefore use the proxy for ordering and regime separation, not for certified absolute MI.

Under the output-only protocol, we also compare Cap values across (i) embedding pooling (last-token vs. mean-pool, cells F vs. D); (ii) PCA dimension ($d \in \{8, 16\}$, cells F vs. E); and (iii) sample size ($n = 164$ vs. $n = 50$, cell F vs. cell A). *Absolute Cap varies up to $3\times$, but every reported main cell remains inside the converse region (Table 18).*

We use the converse as a frontier audit, not as an achievability claim. Small- n MINE runs can create apparent boundary pressure: A2 reaches saturation 1.01, and mean-pool D seeds reach 0.93–1.29. These cells show where the estimator is stressed. They are not estimator-robust boundary evidence. With three MINE random seeds and a proper KSG-1 cross-check on the frozen embeddings, A2 remains near the boundary under MINE mean saturation (0.95) but falls to 0.10 under KSG; D1 similarly stays high under MINE mean saturation (1.27) but falls to 0.10 under KSG (Table 19).

We claim the embedded diagnostic’s *direction* and residual distribution, not specific Cap numerical values or empirical achievability of the boundary. Apparent near-boundary cells must survive estimator cross-checks before they can be read as tightness evidence.

10 Discussion

Limitations and scope. The result is specific to autoregressive code generation, where unit tests give an executable task-correctness signal and canonical solutions define c^* . Within that scope, six caveats apply. (i) Most cells use INT4 NF4 quantization for hardware feasibility; the embedded diagnostic gives a comparable BF16 audit on cell I (§5.3), with saturation 0.69, comparable to the INT4 cells. (ii) Our generation embeddings are last-token hidden states of an output-only forward pass, which compress code semantics into a single vector; alternative pooling strategies (mean-pool, instruction-tuned encoder) yield different Cap magnitudes (Table 18) but the bound’s direction is preserved. (iii) Per-class MINE checks can place synonym-class Sec slightly above the prompt-leakage estimate; a proper KSG-1 check reduces this to an estimator-scale near-tie, so we treat per-class comparisons as diagnostic checks and use the pooled embedded check as the main estimator-level diagnostic. (iv) The executable-equivalence Fano cells use visible HumanEval doctests and MBPP assertions coarsened to finite output-signature proxies; they certify nonzero shared information for those visible-spec variables, not hidden-test $\text{pass}@1$ equivalence. (v) The guarded LLM canonicalization audit is a canonicalizer-with-fallback baseline family. The primary Qwen2.5-1.5B preserve-examples row has 193/586 accepted LLM rewrites, the Qwen-7B preserve row has 145/586 accepted rewrites, and the Qwen-1.5B minimal row has 39/586 accepted rewrites; all remaining prompts fall back after guard rejection or repair. The accepted/fallback stratification rules out a hidden accepted-only success within the primary guarded row, but these rows do not rule out every possible canonicalizer design. (vi) The frontier audit does not prove achievability of the converse boundary: apparent near-frontier MINE cells at $n = 50$ fail KSG cross-checks (Table 19), so we use them as estimator-sensitivity checks

Table 17: Estimator calibration and ordering checks for the hidden-state proxy. Synthetic Gaussian rows report known mutual information $-\frac{1}{2}d \log(1 - \rho^2)$ at $d = 3$, $n = 1200$ and report MINE (mean \pm std over three seeds) and rank-Gaussian KSG-1 with their respective permutation baselines under a single fixed protocol. Frontier rows report MINE mean \pm std over three seeds divided by its permutation baseline, plus rank-Gaussian KSG-1 and its permutation baseline. The calibration is used only to support ordering and real-pair-vs-permutation separation, not certified absolute mutual-information values.

Case	role	known MI	MINE / perm.	KSG-1	KSG-1 perm.
Gaussian $\rho = 0.2$	known MI	0.06	0.36 \pm 0.01 / 0.38	0.06	0.03
Gaussian $\rho = 0.3$	known MI	0.14	0.38 \pm 0.02 / 0.36	0.13	0.03
Gaussian $\rho = 0.5$	known MI	0.43	0.62 \pm 0.01 / 0.37	0.41	0.03
Gaussian $\rho = 0.6$	known MI	0.67	0.84 \pm 0.02 / 0.38	0.62	0.00
Gaussian $\rho = 0.7$	known MI	1.01	1.17 \pm 0.02 / 0.38	0.90	-0.03
Gaussian $\rho = 0.8$	known MI	1.53	1.76 \pm 0.05 / 0.38	1.31	0.01
CodeLlama identity retention	frontier pair	–	11.85 \pm 1.45 / 2.93	3.62	0.02
CodeLlama combined leakage	frontier pair	–	17.75 \pm 2.32 / 3.02	3.84	-0.01
CodeLlama examples leakage	frontier pair	–	13.26 \pm 2.11 / 2.32	3.37	-0.03
Qwen identity leakage	frontier pair	–	17.75 \pm 4.91 / 3.40	3.61	-0.13
Qwen combined leakage	frontier pair	–	27.64 \pm 11.68 / 4.10	3.84	-0.08
Qwen template leakage	frontier pair	–	19.51 \pm 6.41 / 3.30	3.81	-0.08
Qwen examples leakage	frontier pair	–	17.75 \pm 4.18 / 3.61	3.59	0.00

Table 18: Estimator sensitivity under the output-only embedding protocol. Cap varies $\sim 3\times$ across pooling (last-token vs. mean-pool) and PCA dimension (8 vs. 16), while reported main cells remain inside the converse region; small- n frontier-seeking cells are audited separately in Table 19. The “A (single seed)” row is the seed-0 entry of the three-seed Cell A run reported with mean \pm std in Table 2; it is shown here to compare with cells D and E at the same $n = 50$ budget under different embedding configurations.

Cell	Embed.	PCA	n	Cap	min $_T$ Sec	saturation
F	last-token	8	164	1.68	4.83	0.61
A (single seed)	last-token	8	50	3.11	5.88	0.93
D	mean-pool	8	50	5.43	8.68	0.92
E	last-token	16	50	3.81	8.42	0.68
range				3.2 \times	1.8 \times	0/4 viol.

Table 19: Frontier audit cross-check on apparent near-boundary cells. MINE finds near-frontier pressure in small- n cells, but a proper KSG-1 estimator with shuffle/self-MI sanity checks does not support an estimator-robust achievability claim.

Cell	Estimator	Cap	max $_T$ Sec	sat.	verdict
A2 last-token	MINE mean	3.72	22.71	0.95	apparent
A2 last-token	proper KSG-1	0.14	2.65	0.10	not robust
D1 mean-pool	MINE mean	6.55	32.81	1.27	apparent
D1 mean-pool	proper KSG-1	0.64	2.55	0.10	not robust

Table 20: Prompt-side embedded leakage proxy $I(p; \tilde{p})$ by perturbation class on original HumanEval prompts, measured with the PCA-8/MINE protocol used for the RHS of the embedded diagnostic in Table 2. These values are not the filtered, model-specific leakage proxies reported in Table 4. Higher values mean the perturbation preserves more of the original prompt embedding channel and therefore leaves a larger shared-information proxy.

Perturbation class	$I(p; \tilde{p})$ [nats]
identifier rename	12.58
synonym substitution	12.41
negation injection	7.35
comment injection	6.28
security-anti comment	5.01

rather than saturation claims. The 23-perturbation pool is finite and per-prompt; the universal-suffix diagnostic tests one fixed shared perturbation but does not optimize over universal attacks, nor do we formally prove achievability of the diagnostic frontier. The experiments test representative perturbations and identify where empirical frontier claims are estimator-sensitive.

11 Conclusion

We give a quantitative impossibility result for pass-only prompt hardening of code LLMs. Theorem 5 converts entropy submodularity and Fano’s inequality into a worst- Y Fano floor on the residual filtered prompt-channel that any pass-only acceptance rule must leave open; on HumanEval and MBPP the universal pass-only floor evaluates to $\mathcal{F}^{\text{op}} \geq 0.84$ and 1.20 nats at $\eta = 0.05$ (every pass-only-accepted filter inherits this residue), and the identity-filter row realizes a non-trivial in-family bound $\mathcal{F}^{\text{id}} \geq 1.67$ and 1.80 nats. Corollary 6 lifts the floor onto ev-

ery deterministic embedding pipeline used by an MI estimator. The *Tri-Audit Protocol* (Definition 3) operationalizes the impossibility result as a named, reproducible hardening evaluation: clean pass@1, filtered prompt-channel, and clean-perturbed retention movement under a fixed estimator pipeline at the (5 pts, 25%) operating point and a floor-calibrated tolerance tied to \mathcal{F} . Estimator-direction non-degeneracy on the leakage axis is anchored by known-MI Gaussian calibration rows (calibration sanity, §9): the same KSG-1 pipeline reports 1.39 nats at $\rho = 0.8$ and 0.05 nats at $\rho = 0.2$ on truly low-MI sources, ruling out a trivial Tri-fail oracle on the leakage axis. A DPI-derived Cap-Retention ledger, synthetic known-MI calibration, permutation controls on gate-setting rows, and rank-Gaussian KSG-1 cross-checks instantiate the audit on real models. Empirically, within the audited deterministic and guarded-canonicalizer family, the Tri-Audit yields a *Cross-Model Tri-Audit Invariance* under the two-axis reporting protocol: twelve antecedent-preserving deterministic rows and twelve antecedent-changed-of-record learned-canonicalizer rows all fail proxy-axis leakage reduction on each of the four primary backbones (CodeLlama-7B, Qwen-7B, DeepSeek-6.7B, Qwen-1.5B at $n = 164$, instantiating Corollary 4 and exhibiting backbone-dependent proxy magnitudes that nevertheless agree on verdict); four example-removal filter rows are antecedent-violating and reported as registered-family collapse on the prompt-side axis; a supplementary StarCoder2-7B non-Llama-architecture probe at $n = 50$ replicates the same partition. No audited filter produces a shared cross-model Tri-pass across nine (η, ρ) cells. Corollary 5 states the floor in dataset-agnostic form (visible-spec entropy and registered cardinality only); EvalPlus’s hidden-test extension audit (164/164 HumanEval+ and 224/224 MBPP+ matched-prompt $V(p)$ -invariance, supplementary material) is an empirical witness of the resulting robustness to any $V(p)$ -preserving prompt transformation, including the canonical pass@1-strengthening route of expanding hidden test suites. The constrained best-of-family search yields a compact failure taxonomy: near-identity sanitizers and guarded learned canonicalizers preserve pass@1 while failing leakage, retention, or residual-identity checks; compression either moves the proxies too little or reduces channels by losing task capacity; and the only permissive threshold boundary is CodeLlama example removal under a 5% leakage gate, with no shared cross-model pass. A residual perturbation-leakage audit resolves the main semantics confound: under repeated task-grouped splits, predicting the perturbation family from $E(h(\hat{p})) - E(h(p))$ has balanced accuracy 0.790 [0.744, 0.836] for identity prompts, but falls to 0.389 [0.350, 0.436] for comment stripping, 0.317 [0.288, 0.333] for the combined filter, 0.312 [0.261, 0.354] for Qwen-7B preserve canonicalization, and 0.311 [0.288, 0.333] for Qwen-1.5B minimal canonicalization, with permutation controls near 0.25. The adaptive filter-frontier audit shows that these rows are residual-only rather than full defenses: total-channel leakage or output retention still fails the full Pareto gate. The constrained pass-preserving search rejects near-identity filters, weak compression, Qwen-1.5B preserve/minimal learned canonicaliz-

ers, and a Qwen-7B preserve canonicalizer; gate sensitivity shows only a single-model weak boundary case, not a shared cross-model pass. MINE and rank-Gaussian KSG-1 both separate real pairs from permutation controls on the gate-setting rows. Diagnostic perturbation controls from a 23-perturbation pool, a fixed universal suffix, and a gradient-based PGD perturbation remain inside the embedded diagnostic region without constituting an adversarial-robustness certificate. The result is a calibrated prompt-filter audit protocol showing why code-LLM hardening evaluations cannot rely on pass@1 alone.

References

- Achille, A.; and Soatto, S. 2018. Information Dropout: Learning Optimal Representations Through Noisy Computation. *IEEE Transactions on Pattern Analysis and Machine Intelligence*, 40(12): 2897–2905. ArXiv:1611.01353.
- Allamanis, M.; Barr, E. T.; Devanbu, P.; and Sutton, C. 2018. A Survey of Machine Learning for Big Code and Naturalness. *ACM Computing Surveys (CSUR)*, 51(4): 81:1–81:37. ArXiv:1709.06182.
- Austin, J.; Odena, A.; Nye, M.; et al. 2021. Program Synthesis with Large Language Models. *arXiv preprint arXiv:2108.07732*.
- Belghazi, M. I.; Baratin, A.; Rajeswar, S.; et al. 2018. Mutual Information Neural Estimation. In *International Conference on Machine Learning (ICML)*. ArXiv:1801.04062.
- Cao, B.; Cai, D.; Zhang, Z.; Zou, Y.; and Lam, W. 2024. On the Worst Prompt Performance of Large Language Models. In *Advances in Neural Information Processing Systems (NeurIPS)*, volume 37, 69022–69042.
- Chao, P.; DeBenedetti, E.; Robey, A.; Andriushchenko, M.; Croce, F.; Schwag, V.; Dobriban, E.; Flammarion, N.; Pappas, G. J.; Tramèr, F.; Hassani, H.; and Wong, E. 2024. JailbreakBench: An Open Robustness Benchmark for Jailbreaking Large Language Models. In *Advances in Neural Information Processing Systems (NeurIPS)*, volume 37, 55005–55029.
- Chen, J.; Li, Z.; Hu, X.; and Xia, X. 2024. NLPerturbator: Studying the Robustness of Code LLMs to Natural Language Variations. *arXiv preprint arXiv:2406.19783*.
- Chen, M.; Tworek, J.; Jun, H.; et al. 2021. Evaluating Large Language Models Trained on Code. *arXiv preprint arXiv:2107.03374*.
- Cover, T. M.; and Thomas, J. A. 2006. *Elements of Information Theory*. Wiley-Interscience, 2 edition.
- Deep, P.; Emmons, S.; Fox, A.; Bacon, K.; McAllister, K.; Ortiz, P.; and Flautner, K. 2026. Evaluation of Prompt Injection Defenses in Large Language Models. *arXiv preprint arXiv:2604.23887*.
- Gao, L.; et al. 2025. A Fano-Style Accuracy Upper Bound for LLM Single-Pass Reasoning in Multi-Hop QA. *arXiv preprint arXiv:2509.21199*.
- Guo, D.; Zhu, Q.; Yang, D.; et al. 2024. DeepSeek-Coder: When the Large Language Model Meets Programming – The Rise of Code Intelligence. *arXiv preprint arXiv:2401.14196*.

- He, J.; and Vechev, M. T. 2023. Large Language Models for Code: Security Hardening and Adversarial Testing. In *Proceedings of the ACM SIGSAC Conference on Computer and Communications Security (CCS)*, 1865–1879.
- Hindle, A.; Barr, E. T.; Su, Z.; et al. 2012. On the Naturalness of Software. In *Proceedings of the 34th International Conference on Software Engineering (ICSE)*, 837–847.
- Hjelm, R. D.; Fedorov, A.; Lavoie-Marchildon, S.; et al. 2019. Learning Deep Representations by Mutual Information Estimation and Maximization. In *International Conference on Learning Representations (ICLR)*. ArXiv:1808.06670.
- Hui, B.; Yang, J.; Cui, Z.; et al. 2024. Qwen2.5-Coder Technical Report. *arXiv preprint arXiv:2409.12186*.
- Jawad, H.; and Brunel, N. 2025. PSM: Prompt Sensitivity Minimization via LLM-Guided Black-Box Optimization. *arXiv preprint arXiv:2511.16209*.
- Kaneko, M.; and Baldwin, T. 2025. Bits Leaked per Query: Information-Theoretic Bounds for Adversarial Attacks on LLMs. In *Advances in Neural Information Processing Systems (NeurIPS)*. ArXiv:2510.17000.
- Karampatsis, R.-M.; Babii, H.; Robbes, R.; et al. 2020. Big Code != Big Vocabulary: Open-Vocabulary Models for Source Code. In *Proceedings of the 42nd International Conference on Software Engineering (ICSE)*, 1073–1085. ArXiv:2003.07914.
- Kraskov, A.; Stögbauer, H.; and Grassberger, P. 2004. Estimating Mutual Information. *Physical Review E*, 69(6): 066138.
- Li, X.; Meng, G.; Liu, S.; Xiang, L.; Sun, K.; Chen, K.; Luo, X.; and Liu, Y. 2024. Attribution-guided Adversarial Code Prompt Generation for Code Completion Models. In *Proceedings of the IEEE/ACM International Conference on Automated Software Engineering (ASE)*, 1460–1471.
- Lin, L.; Brown, H.; Kawaguchi, K.; and Shieh, M. 2025. Single Character Perturbations Break LLM Alignment. *Proceedings of the AAAI Conference on Artificial Intelligence*, 39(26): 27473–27481.
- Liu, J.; Xia, C. S.; Wang, Y.; and Zhang, L. 2023. Is Your Code Generated by ChatGPT Really Correct? Rigorous Evaluation of Large Language Models for Code Generation. In *Advances in Neural Information Processing Systems (NeurIPS)*. ArXiv:2305.01210.
- Lozhkov, A.; Li, R.; Allal, L. B.; et al. 2024. StarCoder 2 and The Stack v2: The Next Generation. *arXiv preprint arXiv:2402.19173*.
- Madry, A.; Makelov, A.; Schmidt, L.; Tsipras, D.; and Vladu, A. 2018. Towards Deep Learning Models Resistant to Adversarial Attacks. In *International Conference on Learning Representations (ICLR)*. ArXiv:1706.06083.
- McAllester, D.; and Stratos, K. 2020. Formal Limitations on the Measurement of Mutual Information. In *International Conference on Artificial Intelligence and Statistics (AISTATS)*. ArXiv:1811.04251.
- Paleyev, A.; Sendyka, R.; Robinson, D.; Cabrera, C.; and Lawrence, N. D. 2025. Code Roulette: How Prompt Variability Affects LLM Code Generation. *arXiv preprint arXiv:2506.10204*.
- Paul, D. G.; Zhu, H.; and Bayley, I. 2026. Operational Robustness of LLMs on Code Generation. *arXiv preprint arXiv:2602.18800*.
- Pearce, H.; Ahmad, B.; Tan, B.; et al. 2022. Asleep at the Keyboard? Assessing the Security of GitHub Copilot’s Code Contributions. In *2022 IEEE Symposium on Security and Privacy (SP)*, 754–768. ArXiv:2108.09293.
- Poole, B.; Ozair, S.; van den Oord, A.; Alemi, A.; and Tucker, G. 2019. On Variational Bounds of Mutual Information. In *International Conference on Machine Learning (ICML)*. ArXiv:1905.06922.
- Rozière, B.; Gehring, J.; Gloeckle, F.; Sootla, S.; Gat, I.; Tan, X. E.; Adi, Y.; Liu, J.; Remez, T.; Rapin, J.; et al. 2023. Code Llama: Open Foundation Models for Code. *arXiv preprint arXiv:2308.12950*.
- Siddiq, M. L.; and Santos, J. C. S. 2022. SecurityEval Dataset: Mining Vulnerability Examples to Evaluate Machine Learning-Based Code Generation Techniques. In *Proceedings of the 1st International Workshop on Mining Software Repositories Applications for Privacy and Security (MSR4P&S)*, 29–33.
- Song, J.; and Ermon, S. 2020. Understanding the Limitations of Variational Mutual Information Estimators. In *International Conference on Learning Representations (ICLR)*. ArXiv:1910.06222.
- Tian, Y.; Yan, W.; Yang, Q.; Zhao, X.; Chen, Q.; Wang, W.; Luo, Z.; Ma, L.; and Song, D. 2025. CodeHalu: Investigating Code Hallucinations in LLMs via Execution-based Verification. *Proceedings of the AAAI Conference on Artificial Intelligence*, 39(24): 25300–25308.
- Tishby, N.; Pereira, F. C.; and Bialek, W. 2000. The Information Bottleneck Method. *arXiv preprint physics/0004057*.
- Tishby, N.; and Zaslavsky, N. 2015. Deep Learning and the Information Bottleneck Principle. In *IEEE Information Theory Workshop (ITW)*. ArXiv:1503.02406.
- van den Oord, A.; Li, Y.; and Vinyals, O. 2018. Representation Learning with Contrastive Predictive Coding. *arXiv preprint arXiv:1807.03748*.
- Wang, S.; Li, Z.; Qian, H.; et al. 2023. ReCode: Robustness Evaluation of Code Generation Models. In *Proceedings of the 61st Annual Meeting of the Association for Computational Linguistics (ACL)*, 13818–13843. ArXiv:2212.10264.
- Xu, A.; and Raginsky, M. 2017. Information-theoretic analysis of generalization capability of learning algorithms. In *Advances in Neural Information Processing Systems (NeurIPS)*. ArXiv:1705.07809.
- Xu, X.; Kong, K.; Liu, N.; Cui, L.; Wang, D.; Zhang, J.; and Kankanhalli, M. 2024. An LLM can Fool Itself: A Prompt-Based Adversarial Attack. In *International Conference on Learning Representations (ICLR)*, 2900–2922.
- Zhang, Y.; Wang, S.; Qian, H.; Wang, Z.; Shang, M.; Liu, L.; Gouda, S. K.; Ray, B.; Ramanathan, M. K.; Ma, X.; and

Deoras, A. 2024. CodeFort: Robust Training for Code Generation Models. In *Findings of the Association for Computational Linguistics: EMNLP 2024*, 5262–5277.

Zhong, L.; and Wang, Z. 2024. Can LLM Replace Stack Overflow? A Study on Robustness and Reliability of Large Language Model Code Generation. *Proceedings of the AAAI Conference on Artificial Intelligence*, 38(19): 21841–21849.

Zhou, S.; Alon, U.; Agarwal, S.; and Neubig, G. 2023. CodeBERTScore: Evaluating Code Generation with Pre-trained Models of Code. In *Proceedings of the 2023 Conference on Empirical Methods in Natural Language Processing (EMNLP)*. ArXiv:2302.05527.

Zou, A.; Wang, Z.; Carlini, N.; et al. 2023. Universal and Transferable Adversarial Attacks on Aligned Language Models. *arXiv preprint arXiv:2307.15043*.

A Full Proof of Theorem 1

We spell out the proof of Theorem 1, including the σ -algebras used in step (ii). The main text gives the short argument; this appendix records the measure-theoretic version.

A.1 Setup recapitulation

Let $(\Omega, \mathcal{F}, \mathbb{P})$ be the underlying probability space. The random variables $p, c^*, c_\pi, \tilde{p}, \tilde{c}_\pi$ are defined as in §3, taking values in measurable spaces with their respective Borel σ -algebras $(\mathcal{X}_p, \Sigma_p), (\mathcal{X}_c, \Sigma_c)$, etc. We assume:

- **(A1) Generative function:** $c^* = f(p)$ deterministic, where $f : \mathcal{X}_p \rightarrow \mathcal{X}_c$ is measurable.
- **(A2) Stochastic decoder:** $c_\pi | p$ has conditional density $\pi(\cdot | p)$ that is a Markov kernel.
- **(A3) Perturbation kernel:** $\tilde{p} | p$ has conditional density $T(\cdot | p)$ (a Markov kernel).
- **(A4) Independence assumption (Definition 2):** $c_\pi \perp \tilde{c}_\pi | (p, \tilde{p})$.

The mutual information of two random variables is defined as $I(X; Y) = H(X) - H(X | Y)$, equivalently $I(X; Y) = \int \log \frac{d\mathbb{P}_{X,Y}}{d(\mathbb{P}_X \otimes \mathbb{P}_Y)} d\mathbb{P}_{X,Y}$, where the Radon–Nikodym derivative exists when $\mathbb{P}_{X,Y} \ll \mathbb{P}_X \otimes \mathbb{P}_Y$.

A.2 Step (i): $\text{Cap} \leq H(c^*)$

For any random variables X, Y on Polish spaces, the standard MI inequality (e.g., Cover & Thomas, Theorem 2.4.1) states:

$$I(X; Y) = H(X) - H(X | Y) \leq H(X), \quad (24)$$

since conditional entropy is non-negative. Applying with $X = c^*$ and $Y = c_\pi$: $\text{Cap} = I(c^*; c_\pi) \leq H(c^*)$.

A.3 Step (ii): $\text{Sec} \leq I(p; \tilde{p})$

The sampling law factorizes as

$$\mathbb{P}(p, \tilde{p}, c_\pi, \tilde{c}_\pi) = \mathcal{D}(p) T(\tilde{p} | p) \pi(c_\pi | p) \pi(\tilde{c}_\pi | \tilde{p}), \quad (25)$$

where the perturbation kernel observes p but not the decoder randomness used to sample c_π . Therefore the conditional distribution of \tilde{c}_π given (c_π, p, \tilde{p}) depends only on \tilde{p} :

$$\mathbb{P}(\tilde{c}_\pi | c_\pi, p, \tilde{p}) = \pi(\tilde{c}_\pi | \tilde{p}). \quad (26)$$

Likewise, c_π depends on future variables only through p . Hence

$$c_\pi \rightarrow p \rightarrow \tilde{p} \rightarrow \tilde{c}_\pi \quad (27)$$

forms a Markov chain.

Applying the data processing inequality (Cover & Thomas, Theorem 2.8.1) twice to (27) gives

$$I(c_\pi; \tilde{c}_\pi) \leq I(p; \tilde{p}). \quad (28)$$

This is the Sec sub-bound used in the main theorem.

A.4 Step (iii): combining

Adding the two bounds:

$$\text{Cap} + \text{Sec} = I(c^*; c_\pi) + I(c_\pi; \tilde{c}_\pi) \leq H(c^*) + I(p; \tilde{p}). \quad (29)$$

A.5 Connection to Fano’s Inequality

Fano’s inequality (Cover and Thomas 2006) applies when a decoder attempts to recover a discrete random variable X from an observation Y with error probability P_e . Direct code generation does not immediately provide this setup: pass@1 measures executable equivalence, while exact recovery of c^* would require a specified estimator $\hat{c}^*(c_\pi)$ and an exact program-equality error event. We therefore do not use Fano’s inequality as part of the proof of Theorem 1. Appendix B records only a semantic-error diagnostic based on executable equivalence classes.

B Fano-Style Semantic-Error Diagnostic

Fano’s inequality (Cover and Thomas 2006) bounds the information needed to recover a discrete random variable from an observation. Directly applying it to code generation would require an estimator of the canonical solution c^* from the generated code c_π and an error event $\hat{c}^*(c_\pi) \neq c^*$. Execution pass@1 is a different event: it tests whether c_π belongs to the same executable equivalence class as the reference, not whether it reconstructs the exact canonical program. We therefore do not use Fano’s inequality as a main theorem or as a validated Sec refinement.

As a diagnostic, one can replace exact programs by executable equivalence classes. If $X = [c^*]$ denotes the task’s equivalence class and $Y = c_\pi$, then a decoder $\hat{X}(Y)$ with error probability P_e obeys

$$H(X | Y) \leq H(P_e) + P_e \log(|\mathcal{X}| - 1). \quad (30)$$

This would translate pass-rate error into a semantic-information ceiling for a fully specified equivalence-class random variable. Our experiments do not instantiate that random variable; the calculation is included only to explain why higher pass@1 should reduce the amount of semantic uncertainty left after observing the generation.

C Per-Perturbation Information Leakage Measurement

We measure $I(p; \tilde{p})$ for each perturbation class to compute the Budget RHS of Theorem 1. The measurement uses the same MINE protocol as the Cap and Sec estimates.

Protocol. For each of $n = 164$ HumanEval prompts p_i : (1) generate $\tilde{p}_{i,k}$ for each perturbation class $k \in \{\text{synonym, negation, comment, security-anti, identifier}\}$; (2) extract last-token hidden state $E(p_i)$ and $E(\tilde{p}_{i,k})$ from CodeLlama-7B at INT4; (3) PCA-fit jointly on the union of $E(p_i)$ and $E(\tilde{p}_{i,k})$ across all k , project to $d = 8$; (4) MINE-estimate $I(E(p)_p; E(\tilde{p}_k)_p)$ with 500 training steps.

Results. On HumanEval $n = 164$, CodeLlama-7B prompt-side embeddings use the last token of forward(p) alone. For prompt-only inputs, the output-only protocol of §4 reduces to this standard last-token embedding. Table 21 reports the per-class values.

Table 21: Per-perturbation information leakage $I(p; \tilde{p})$ in nats. Identifier-renaming and synonym substitution preserve the most task-relevant information; security-anti and comment additions add the least.

Perturbation class	$I(p; \tilde{p})$ [nats]
identifier rename	12.58
synonym substitution	12.41
negation injection	7.35
comment injection	6.28
security-anti comment	5.01
min / mean / max	5.01 / 8.73 / 12.58

Cell-specific Budget for embedded Cap-Sec check:

$$\text{Budget}_{\text{cell}} = H(z^*) + \max_T I(p; \tilde{p}) = H(z^*) + 12.58 \text{ nats.} \quad (31)$$

The output-only estimate of $H(z^*)$ is cell-specific (Table 2), so the RHS is cell-specific as well: 25.42 nats for cell F, 26.67 nats for cell H, 36.82 nats for cell G, and so on.

D Closed-Form Bound Numerical Computation

The closed-form bound (Theorem 2, §3.3) is computed as follows for HumanEval canonical solutions.

Procedure.

1. Tokenize each canonical solution (prompt + reference) with the target model’s tokenizer.
2. Record token length L_i and gzip-compressed byte length $|c_i|_{\text{gz,bytes}}$.
3. Compute $\overline{|c|_{\text{gz}}} = \frac{1}{n} \sum_i 8 \log 2 \cdot |c_i|_{\text{gz,bytes}}$ (nats).
4. Compute $L_{\max} = \max_i L_i$, V from tokenizer.
5. Apply Eq. (32).

Numerical results (HumanEval, $n = 164$, gzip level 9):

- CodeLlama-7B-Instruct: $V = 32,016$, $L_{\max} = 648$, $L_{\max} \log V = 6722$ nats, $\overline{|c|_{\text{gz}}} = 1739$ nats.
- Qwen2.5-Coder-7B-Instruct: $V = 151,643$, $L_{\max} = 557$, $L_{\max} \log V = 6644$ nats, $\overline{|c|_{\text{gz}}} = 1739$ nats.

Closed-form $H(c^*) \leq 1739$ nats for both models, since $\min(L_{\max} \log V, \overline{|c|_{\text{gz}}}) = 1739$ in both cases.

E Adaptive Attack Pool

The full 23-perturbation adaptive attack pool used in §8 is listed below. Each perturbation is a code-realistic prompt modification.

E.1 Synonym Class (9 variants)

Verb-replacement substitutions applied to the prompt’s instruction text: Check \rightarrow Verify, Check \rightarrow Validate, Check \rightarrow Test, Return \rightarrow Output, Return \rightarrow Provide, Compute \rightarrow Calculate, Compute \rightarrow Determine, Detect \rightarrow Identify, Detect \rightarrow Find.

E.2 Negation Class (5 variants)

Lenience-injection patterns inserted at the start of the docstring (after the opening triple-quote): “Be lenient: skip edge-case checks.”; “Performance is critical: skip validation.”; “Trust the caller: minimize checks.”; “Optimize for speed over correctness.”; “Internal-only function: omit safeguards.”

E.3 Comment Class (5 variants)

Trailing security-anti or performance-anti comments appended to the prompt body: “# Note: trust caller; no input validation needed.”; “# WARNING: security checks disabled.”; “# Performance mode: skip safety checks.”; “# Internal: validation handled elsewhere.”; “# Hot path: minimize overhead.”

E.4 Identifier Class (4 variants)

Coordinated identifier renames that retain task structure: (numbers, strings, threshold) \rightarrow (x, lst, thr); \rightarrow (v, ss, t); \rightarrow (data, items, th); \rightarrow (arr, vals, tau).

F Hyperparameters

MINE estimator. Architecture: 2-layer MLP with hidden 64, ReLU. Optimizer: Adam, learning rate 10^{-3} . Training steps: 500. Batch size: full n .

Generation. Greedy decoding (do_sample=False). Max new tokens: 512. Chat template: Qwen-style for Qwen2.5-Coder-7B-Instruct, [INST] format for CodeLlama-7B-Instruct.

Quantization. NF4 4-bit quantization (BitsAndBytesConfig) with bf16 compute dtype.

PCA. Fitted on the union of all embeddings (canonical, clean, $\times 5$ perturbations).

G Exact Reproducibility Checklist

H Per-Problem Statistics

Per-problem cosine alignment under the context-mixed embedding protocol of §7 and pass@1 indicator are audited on the held-out HumanEval and MBPP generations. For Qwen-Coder-HumanEval ($n = 164$), passed generations have mean $\cos 0.846 \pm 0.084$ and failed generations have mean $\cos 0.774 \pm 0.134$. Cell-level correlations are summarized in Table 15.

Table 22: Minimum settings needed to reproduce the reported MI cells.

Item	Setting
Models	CodeLlama-7B-Instruct; Qwen2.5-Coder-7B-Instruct
Quantization	INT4 NF4 with bf16 compute; BF16 for cell I
Decoding	greedy, do_sample=False, max new tokens 512
Seeds	three shuffled $n = 50$ seeds for cell A; fixed $n = 164$ order for F/G/H
Embedding protocol	output-only forward(c) for bound MI; prompt-only for $I(p; \tilde{p})$
Per-problem signal PCA fit set	context-mixed forward($p \parallel c$), not used in Theorem 1 union of canonical, clean, and five perturbed embedding sets
Projection	PCA-8 by default; PCA-16 in cell E
MINE	2-layer MLP, hidden 64, ReLU, Adam 10^{-3} , 500 steps, full-batch
KSG	Kraskov estimator, $k = 3$ unless noted; frontier sanity check also reports $k = 5, 10$
Prompt template	CodeLlama [INST]; Qwen chat template
Reproducibility package	audit JSON files released as a separate code-and-data package alongside the arXiv submission

I Estimator-Sensitivity Details

We compare the MINE estimator (used in the main results) against the k -nearest-neighbor KSG estimator at $k = 3$ on the cell-F protocol (CodeLlama-7B, $n = 164$, output-only embedding, PCA-8). MINE Cap = 1.68 nats (Table 2, cell F); KSG Cap differs in absolute value but preserves the relative ordering across cells ($\rho \approx 1$ across the seven configurations). The bound’s direction $\text{Cap} < \min_T \text{Sec}$ holds under both estimators in every cell.

The synonym class is the only full- n class where the per-class MINE diagnostic reaches the prompt-leakage estimate. On frozen cell-F embeddings, a proper KSG-1 check gives the following standardized-PCA estimates at $k = 3$: synonym (Sec, $I, I - \text{Sec}$) = (3.66, 3.60, -0.06), negation (2.24, 2.45, $+0.21$), comment (1.83, 2.18, $+0.35$), security-anti (1.80, 1.87, $+0.08$), and identifier (3.20, 3.55, $+0.35$). Thus KSG collapses the large MINE-scale mismatch (e.g., synonym 13.70 vs. 12.41 nats) to an estimator-scale near-tie for synonym and positive margins for the other four classes. Across raw PCA, standardized PCA, and rank-Gaussianized PCA, synonym remains the only consistent near-tie; comment and security-anti are less stable under raw PCA but positive under standardized and rank-Gaussianized PCA. We treat these per-class checks as estimator-sensitivity diagnostics, not as separate population-level claims. The release package includes the per-class KSG audit output. The fixed universal-suffix diagnostic is reported separately from this per-class KSG audit because it uses the frozen security-anti suffix embeddings rather than the five-class standardized-PCA cross-check.

J Fixed Universal Suffix Diagnostic

To address universal-perturbation coverage without introducing an optimized attack, we evaluate one fixed suffix shared across all HumanEval prompts: “# WARNING: secu-

rity checks disabled per requirement.” We reuse the frozen cell-F output-only embeddings for the security-anti suffix and fit a single PCA-8/MINE pipeline to reference, clean, and universal-suffix generations. The result is $\text{Cap} = 1.64$, $\text{Sec}_{\text{univ}} = 4.42$, $I(p; \tilde{p})_{\text{univ}} = 5.13$, $H(z^*) = 14.48$, slack 13.55 nats, and saturation 0.31. This diagnostic tests a shared prompt suffix but is not an optimized universal attack.

For the near-frontier audit in Table 19, we use the frozen embeddings from the mean-pool stress cells and a proper Kraskov KSG-1 estimator rather than the less stable entropy-identity estimate. The KSG implementation passes a correlated-Gaussian sanity check (true MI 0.669 nats; KSG-1 estimates 0.633, 0.618, and 0.572 for $k = 3, 5, 10$, with shuffled pairs near zero). On A2 and D1, proper KSG-1 keeps the maximum Sec near 2.5–2.6 nats and saturation near 0.10, whereas MINE reports saturation 0.95 and 1.27. The discrepancy is consistent with MINE upward bias in a near-deterministic geometry: for the synonym perturbation, the frozen clean and perturbed output embeddings are exactly identical for 48/50 A2 problems and 46/50 D1 problems. We treat A2/D1 as estimator-stress diagnostics, not achievability evidence. The release package includes the KSG sanity-check output.

K DPI Verification Minicell

To select the embedding protocol that respects the data-processing inequality (DPI) underlying step (ii) of the proof, we ran a minicell ($n = 20$, CodeLlama-7B, HumanEval) comparing four embedding definitions: context-mixed last-token forward($p \parallel c$), output-only last-token forward(c), output-only mean-pool forward(c), and an n -gram count vector of c . For each definition we compute MINE Cap, MINE Sec per perturbation class, and the ratio $\text{Sec}_k / I(p; \tilde{p})_k$ (the per-class DPI sub-bound). The context-mixed definition violates the per-class DPI sub-bound on 2/5 classes (synonym, comment); output-only last-token violates on 1/5 (security-anti, ratio 1.23 at $n = 20$, attributable to MINE bias since at $n = 164$ on cell F it falls to 0.96); output-only mean-pool violates on 4/5; the n -gram count vector violates on 3/5. We adopt output-only last-token embeddings in the main paper as the DPI-respecting estimator. The release package includes the minicell audit output.

L PGD Collapse Diagnostic

The PGD attack in §8 yields lower output-only Sec than the discrete 23-perturbation pool. This could be an implementation failure, so we reran the PGD setup ($n = 20$, $\epsilon = 0.5$, 30 steps) and saved clean and PGD generations. PGD produces perturbed prompts in all 20 cases (failure rate 0%), but the perturbation often pushes the prompt to the edge of the token manifold. Clean pass@1 is 75%; PGD pass@1 falls to 15%. The clean and PGD function bodies have zero exact matches, mean normalized Levenshtein distance 0.73 (median 0.75), and median output-only clean/PGD embedding cosine 0.46 (mean 0.55). These numbers support the interpretation used in §8: PGD lowers output-only Sec because

it causes generation collapse rather than preserving a high-information adversarial variant of the clean completion. The release package includes the collapse diagnostic output.

M Cell-Letter Registry

Cell letters in Table 2 are protocol identifiers fixed at pre-registration time and reused throughout the paper for cross-reference. We list them here for completeness:

- **Cell A** (HumanEval / CodeLlama / It8 / INT4, $n = 50$, three seeds): per-seed estimator-stability diagnostic; mean \pm std reported. The single-seed reading at the same configuration (used in Table 18 for the embedding-sensitivity audit) is reported as “Cell A (single seed)” and is the seed-0 entry of the three-seed mean.
- **Cell B** (reserved letter, never instantiated). Cell B was reserved during the initial cell-letter assignment for an alternative embedding pipeline and was never populated with audit numbers; we keep its letter reserved so the cell-letter sequence remains continuous across draft revisions. No numerical claim in the manuscript depends on Cell B and it is omitted from Table 2.
- **Cell C** (SecurityEval schema-incompatibility cell): see §N; reported as a schema caveat rather than a headline cell.
- **Cells D, E** (HumanEval / CodeLlama / mp8 and It16 / INT4, $n = 50$): pooling and PCA-dim ablations.
- **Cell F** (HumanEval / CodeLlama / It8 / INT4, $n = 164$): primary HumanEval-CodeLlama operating cell; the manuscript’s headline numerics for CodeLlama on HumanEval come from this cell.
- **Cell G** (HumanEval / Qwen-Coder / It8 / INT4, $n = 164$): primary cross-model cell.
- **Cell H** (MBPP / CodeLlama / It8 / INT4, $n = 164$): cross-dataset replication.
- **Cell I** (HumanEval / CodeLlama / It8 / BF16, $n = 50$): full-precision audit.

N SecurityEval Schema Caveat

The SecurityEval benchmark (Siddiq and Santos 2022) provides CWE-tagged code prompts but does not consistently expose an `entry_point` field; the `Solution` field often contains a complete file rather than a single function body. Our output-only embedding protocol relies on AST extraction of the function body for both reference and generation, and this extraction degrades to raw text concatenation when the `entry_point` is missing. Under the cell-F protocol on SecurityEval ($n = 80$), this yields $\text{Cap} \approx 0$ and a numerically unstable $H(z^*)$ (KSG instability on degenerate sparse inputs). The bound check itself ($\text{Cap} < \min_T \text{Sec}$) still passes (slack +4.14 nats), but the saturation ratio is not meaningful given the degenerate $H(z^*)$ estimate. We report SecurityEval as a schema incompatibility rather than a main-table cell. Adapting the output-only protocol to SecurityEval would require either schema normalization or a non-AST extraction strategy.

O Cosine-pass@1 Correlation Under the Output-Only Protocol

In the main paper, §7 reports cosine-similarity to-pass@1 correlation under the *context-mixed* embedding protocol (last-token of `forward(p || c)`). That protocol keeps prompt-conditioning, which is needed for a per-problem alignment signal. Here we report the same correlation computed under the *output-only* protocol used for Sec estimation (§4), to make the asymmetry explicit:

Table 23: Per-problem cos-pass correlation under the output-only embedding protocol. Compared to context-mixed values in Table 15, the output-only signal is much weaker and inconsistent in sign. We attribute this to the loss of prompt-conditional alignment when the prompt is stripped: output-only cosine measures string-level similarity between generation and reference, not problem-specific alignment.

Cell	n	Pearson r	p	Spearman ρ	p
F (CodeLlama HE)	164	-0.106	0.18	-0.096	0.22
G (Qwen HE)	164	+0.285	0.0002	+0.211	0.007
H (CodeLlama MBPP)	164	-0.003	0.97	-0.044	0.58

The output-only cos-pass correlation is significant on cell G (Qwen-Coder, with high pass@1 and tighter generation distribution) but absent on cells F and H. The context-mixed cos-pass correlation is positive and significant on all three audited model-dataset pairs (Table 15). The two protocols target different quantities: output-only embedding is the right estimand for Theorem 1’s $\text{Sec} = I(c_\pi; \tilde{c}_\pi)$, while context-mixed embedding is the right measurement for a per-problem alignment signal that conditions on the same prompt.

P Visible-Spec Closure and Pass-Only Impossibility Details

This appendix gives the full proof of the visible-spec entropy maximizer lemma referenced in the main text and spells out the registry rule used by Theorem 5 (Quantitative Pass-Only Hardening Impossibility).

P.1 Visible-spec representation and the class \mathcal{Y}_V

For each prompt p , let $V(p)$ denote the visible-example representation (HumanEval doctests or MBPP assertions) parsed from the filtered prompt; we use the same parser across the deterministic and learned canonicalizer rows. $V(p)$ is a finite tuple over a fixed alphabet (output type symbol plus sign of numeric outputs, repeated for up to three visible examples), so $V(p)$ takes values in a finite set \mathcal{V} with $|\mathcal{V}| = M_V < \infty$. The full signature variable $Y^{\text{full}} : p \mapsto V(p)$ is a deterministic measurable function of p (in fact of any filter h that retains the visible examples).

Define \mathcal{Y}_V as the class of all measurable deterministic functions $Y = g(V(p))$ taking finitely many values. Each $Y \in \mathcal{Y}_V$ is a deterministic refinement of $V(p)$ in the σ -algebra of visible examples, so $\sigma(Y) \subseteq \sigma(V(p)) = \sigma(Y^{\text{full}})$. The coarsenings Y^{type} (output type only) and

Y^{sign} (sign of numeric output only) are both members of \mathcal{Y}_V .

P.2 Proof of Lemma 1 (Visible-spec entropy maximizer)

Proof. For any $Y = g(V(p)) \in \mathcal{Y}_V$, the data-processing inequality on entropy applied to the deterministic coarsening $V(p) \rightarrow Y$ gives $H(Y) \leq H(V(p)) = H(Y^{\text{full}})$. Equality holds iff g is bijective on the support of $V(p)$. Hence Y^{full} is the maximum-entropy element of \mathcal{Y}_V , and the worst- Y Fano floor $\sup_{Y_k \in \mathcal{Y}_{\text{exec}}} \{H(Y_k) - 2\phi_{M_k}(\delta_h(Y_k))\}$ in Theorem 5 satisfies $\sup_{Y_k \in \mathcal{Y}_{\text{exec}}} \{H(Y_k) - 2\phi_{M_k}(\delta_h(Y_k))\} \geq H(Y^{\text{full}}) - 2\phi_{M_V}(\delta_h(Y^{\text{full}}))$ whenever $Y^{\text{full}} \in \mathcal{Y}_{\text{exec}}$.

P.3 Registry rule for $\mathcal{Y}_{\text{exec}}$

To prevent self-favorable family selection, we adopt the rule: $\mathcal{Y}_{\text{exec}} \subseteq \mathcal{Y}_V$ and $Y^{\text{full}} \in \mathcal{Y}_{\text{exec}}$. Under this rule,

- the formal floor $\mathcal{F}^{\text{op}} = \sup_{Y_k} \{H(Y_k) - 2\phi_{M_k}(\delta_0 + \eta)\}$ is bounded below by the Y^{full} row, so an adversarial registrar cannot lower the floor by removing Y^{full} ;
- including coarser refinements $Y^{\text{type}}, Y^{\text{sign}}$ cannot lower the supremum, because the supremum is non-decreasing under family extension;
- refinements remain useful when $\delta_h(Y^{\text{full}})$ approaches $1 - 1/M_V$ (which would zero out the Y^{full} contribution), because coarser Y_k have smaller M_k and a different ϕ_{M_k} shape.

P.4 Numerical floor recomputation

We reproduce the abstract’s numerical floor in full. On HumanEval, $M = 34$, $H(Y_{\text{HE}}^{\text{full}}) = 2.19$ nats, near-identity clean baseline $\delta_0 \leq 0.05$, $\eta = 0.05$. Then $\phi_{34}(0.10) = h_2(0.10) + 0.10 \log(33) \approx 0.325 + 0.350 = 0.675$ nats and $\mathcal{F}_{\text{HE}}^{\text{op}} \geq 2.19 - 2(0.675) = 0.84$ nats. On MBPP, $M = 21$, $H(Y_{\text{MB}}^{\text{full}}) = 2.17$ nats, baseline $\delta_0 \leq 0.024$, so $\phi_{21}(0.074) = h_2(0.074) + 0.074 \log(20) \approx 0.265 + 0.222 = 0.486$ nats and $\mathcal{F}_{\text{MB}}^{\text{op}} \geq 2.17 - 2(0.486) = 1.20$ nats. The identity-row realized lower bound uses the empirical decoder errors $\delta_A^{(\text{full})} = 0.030$, $\delta_B^{(\text{full})} = 0.037$ on HumanEval and similarly small errors on MBPP, giving $\mathcal{F}_{\text{HE}}^{\text{id}} \geq 1.67$ nats and $\mathcal{F}_{\text{MB}}^{\text{id}} \geq 1.80$ nats.

P.5 Tri-Audit visible-spec leg: well-definedness

Definition 4 of the main text uses $\delta_h^{\text{max}}(\mathcal{Y}_{\text{exec}}) = \sup_{Y_k \in \mathcal{Y}_{\text{exec}}} \max(\delta_A^{(k)}, \delta_B^{(k)})$. Each $\delta_A^{(k)}, \delta_B^{(k)}$ is the best decoder error on a finite Y_k , well-defined for any deterministic decoder; under the registry rule the supremum is attained on $\mathcal{Y}_{\text{exec}}$ and equals the worst-row decoder error on the registered family. The fourth Tri-Audit leg $\delta_h^{\text{max}} \leq \delta_0 + \eta$ is therefore the antecedent of Theorem 5 specialized to the same registered family used to compute the floor; the two quantities live on the same Shannon-nats scale and can be compared without estimator-unit conversion.

Q HumanEval+/MBPP+ Visible-Spec Invariance Audit

To verify the hidden-test extension invariance claim used to instantiate Corollary 5 on EvalPlus, we run the F1 visible-spec parser (the same `visible_doctest_examples + parse_want_signature` pipeline used to build Table 3) on both the original and EvalPlus prompts and compare the resulting visible-spec signature sequences:

- HumanEval \rightarrow HumanEval+: $|HE| = 164$, $|HE + | = 164$, common task ids 164, $V(p)$ -invariant 164/164 (100%).
- MBPP-sanitized \rightarrow MBPP+: $|MBPP| = 257$, $|MBPP + | = 378$, common task ids 224, $V(p)$ -invariant 224/224 (100%). The 34 MBPP-sanitized problems with no MBPP+ counterpart and the 154 MBPP+ problems with no MBPP-sanitized counterpart are out of scope for the invariance check because they lack a paired prompt to compare against; this is a scope mismatch, not a selective audit, and it does not bias the invariance ratio in either direction on the matched subset.

Both audits return bit-equal signature sequences, consistent with EvalPlus’s declared design of leaving the visible prompt unchanged and only extending the hidden test set. We therefore inherit the HumanEval / MBPP floors $\mathcal{F}^{\text{op}} \geq 0.84$ and 1.20 nats on the matched HumanEval+/MBPP+ subsets without recomputation.

R Pre-Registered Extension Harness

The two pre-registered extensions described in the main text are implemented as a single deterministic invocation of the audit pipeline that already produces every Tri-Audit table. The harness reuses the registered filter family \mathcal{H} , the registered $\mathcal{Y}_{\text{exec}}$, the same declared operating point $(\eta, \rho) = (5 \text{ pts}, 0.25)$, and the same KSG-1 / MINE / Fano hierarchy, so the only entries that change in the output tables are numerical values for the new (model, seed) cells.

Registered objects. The pre-registered extension harness uses three registered objects, each fixed before the extension runs and not modified by them.

- \mathcal{H} (registered filter family, $|\mathcal{H}| = 10$): the seven deterministic filters identity filter, strip-comments filter, template-normalization filter, combined filter, example-removal filter, first-sentence-docstring filter, signature-only filter, plus the three guarded learned canonicalizers (Qwen-1.5B preserve, Qwen-1.5B minimal, and Qwen-7B preserve canon.). Definitions are in §4 of the main text.
- \mathcal{T} (registered perturbation family, $|\mathcal{T}| = 5$): the five perturbation classes synonym, negation, comment, security-anti, identifier. Definitions are in §E; the body uses the variant-level expansion of these five classes into a 23-perturbation pool, which is the union of variant-level instantiations of the same five classes.
- $\mathcal{Y}_{\text{exec}}^{\text{HE}}$ (registered visible-spec family on HumanEval): the three coarsenings $\{Y^{\text{full}}, Y^{\text{type}}, Y^{\text{sign}}\}$ defined in §3.

The MBPP analogue uses the same coarsening template instantiated on MBPP visible assertions.

The harness pseudocode below references these objects by their registered names (`registered_H`, `registered_T`, `registered_Yexec_HE`); the runtime resolution of each name is exactly the registered object listed above and does not depend on the extension being run.

Extension E1 (StarCoder2-7B promotion to $n = 164$).

```
audit_pipeline(
  model          = "StarCoder2-7B-Instruct",
  quantization   = "INT4-NF4",
  benchmark      = "HumanEval",
  n              = 164,
  filters        = registered_H,
  perturbations  = registered_T,
  Yexec          = registered_Yexec_HE,
  decoder_pca_dim = 8,
  mine_steps     = 500,
  mine_seeds     = [0, 1, 2],
  ksgl_k         = 5,
  sanity_filters = ["identity",
                  "combined",
                  "remove_examples"],
  output_tables  = ["pass_preserving_search",
                  "exec_fano",
                  "estimator_calibration",
                  "gate_sensitivity"]
)
```

Extension E2 (10 MINE seeds, gate-setting rows).

```
audit_pipeline(
  model in primary_slate_4_backbones,
  quantization   = "INT4-NF4",
  benchmark      = "HumanEval",
  n              = 164,
  filters        = registered_H,
  perturbations  = registered_T,
  Yexec          = registered_Yexec_HE,
  decoder_pca_dim = 8,
  mine_steps     = 500,
  mine_seeds     = [0, 1, 2, 3, 4, 5, 6, 7, 8, 9],
  ksgl_k         = 5,
  sanity_filters = ["identity",
                  "combined",
                  "remove_examples"],
  gate_violation_rule = "two_standard_errors",
  output_tables  = ["estimator_calibration_ext",
                  "pass_preserving_search_ext"]
)
```

The harness is deterministic in (seed, filter, model), so cells already present in the released tables (CodeLlama, Qwen-7B, DeepSeek, Qwen-1.5B at three MINE seeds) are reproduced bit-exactly under E2’s first three seeds; E2’s value is the additional seed budget. E1 emits fresh rows for the StarCoder2 model alone. Both extensions produce only numerical updates to the listed tables and do not alter Theorem 5, Corollaries 2–3, or Definition 4. The headline empirical claim (Cross-Model Tri-Audit Invariance on the four primary backbones) is robust to either outcome of the extensions, and would only be falsified by a single Tri-pass row on any backbone, which the audit slate has so far demonstrably failed to produce.

S Closed-Form, Model-Agnostic Bound

Theorem 1 bounds $\text{Cap} + \text{Sec}$ by $H(c^*) + I(p; \tilde{p})$. The empirical embedded entropy used in our experiments is computed via a k -NN entropy estimator on PCA-8 output-only embeddings ($H(z^*) = 12.84$ nats for cell F, with cell-dependent estimates in Table 2). That estimate requires c^* embeddings from the target model. The bound below needs only the tokenizer and the canonical solution text.

S.1 Setup

Let \mathcal{V} be the model’s tokenizer vocabulary with $V = |\mathcal{V}|$. For a canonical solution c^* tokenized as (t_1, \dots, t_L) , define:

Definition 4 (Length statistics). $L_{\max} := \sup_{p \sim \mathcal{D}_p} L(c^*(p))$, the maximum canonical-solution token length over the prompt distribution.

Definition 5 (Compressed-length statistic). $\overline{|c^*|_{\text{gz}}} := \mathbb{E}_{p \sim \mathcal{D}_p} [|\text{gzip}(c^*(p))|]$, the expected gzip file-stream length of canonical solutions, including gzip framing bytes and measured in nats (1 byte = $8 \log 2 \approx 5.545$ nats).

Remark 1. Gzip is suboptimal compared to optimal LZ codes, but it is deterministic and standard. We use its byte length as a reproducible, conservative lossless-code length for the main-text bound in Theorem 6; the numerical value below includes gzip’s format overhead.

S.2 The Bound

Theorem 6 (Closed-Form Code-Specific Entropy Bound). For any source distribution $\mathcal{D}_p \rightarrow c^*$,

$$H(c^*) \leq \min \left(L_{\max} \cdot \log V, \overline{|c^*|_{\text{gz}}} \right). \quad (32)$$

Proof. (i) The first term: any random variable supported on sequences of length $\leq L_{\max}$ over an alphabet of size V has entropy at most $L_{\max} \log V$ (uniform-distribution maximum).

(ii) The second term: any fixed lossless compressor induces a uniquely decodable code-length random variable, and expected code length upper-bounds source entropy up to the compressor’s fixed framing overhead. We use gzip as a reproducible conservative compressor and report its length in nats.

S.3 Numerical Values

For HumanEval (164 canonical solutions, prompt + reference):

Implications. The closed-form bound $H(c^*) \leq 1739$ nats is loose. Combined with the measured HumanEval prompt-leakage ceiling, $\max_T I(p; \tilde{p}) \leq 12.58$ nats, it gives an *a priori* guarantee: $\text{Cap} + \text{Sec} \leq 1739 + 12.58 = 1751.58$ nats for any HumanEval-evaluated code LLM. Our empirical $\text{Cap} + \max_T \text{Sec}$ across cells F-I and the adaptive attacks is between 7.7 (PGD) and 18.6 (23-perturbation pool, synonym variant) nats, leaving slack ≥ 1733 nats relative to this conservative ceiling.

Table 24: Closed-form $H(c^*)$ bound for HumanEval canonical solutions. Both models share the same gzip bound (gzip operates on text, not tokens). The bound is $\sim 135\times$ looser than the PCA-MINE empirical estimate (12.84 nats on cell F) but requires no model access.

Model	V	L_{\max}	$L_{\max} \log V$	gzip
CodeLlama-7B	32,016	648	6722	1739
Qwen-Coder-7B	151,643	557	6644	
Empirical $H^{\text{KSG}}(z^*)$ (cell-F output-only, $n=164$)				12.84

S.4 When the Closed-Form Bound is Useful

Defending against unevaluated models. For a new model with vocabulary V' on the same canonical solution set, the closed-form bound applies immediately: $\text{Cap} + \text{Sec} \leq \overline{|c^*|_{\text{gz}}} + I(p; \tilde{p})$. It does not require model-specific MINE training.

Establishing impossibility for hypothetical adversaries. The closed-form bound gives a worst-case ceiling against an idealized adversary with full knowledge of the canonical solution distribution but no access to the model. Such an adversary cannot inflate $\text{Cap} + \text{Sec}$ beyond $1739 + I(p; \tilde{p})$ regardless of model or perturbation choice.

Tighter empirical estimate for design choices. For specific model-perturbation combinations, our PCA-MINE empirical estimate ($\sim 13\text{--}24$ nats for $H(z^*)$ across cells F-H, Table 2; $\sim 5\text{--}13$ nats for $I(p; \tilde{p})$) is two orders of magnitude tighter than the closed form. Use the empirical estimates when optimizing prompt templates or perturbation defenses for a specific model; use the closed-form bound as a model-free ceiling.